IEEE Access
Multidisciplinary | Rapid Review | Open Access Journal

Date of publication xxxx 00, 0000, date of current version xxxx 00, 0000.

Digital Object Identifier 10.1109/ACCESS.2017.DOI

A 5-D multi-stable hyperchaotic two-disk dynamo system with no equilibrium point: Circuit design, FPGA realization and applications to TRNGs and image encryption

SUNDARAPANDIAN VAIDYANATHAN[1], ACENG SAMBAS[2], BASSEM ABD-EL-ATTY[3], AHMED A. ABD EL-LATIF[3,4], ESTEBAN TLELO-CUAUTLE[5], OMAR GUILLÉN-FERNÁNDEZ[6], MUSTAFA MAMAT[7], MOHAMAD AFENDEE MOHAMED[8], MURAT ALÇIN[9], MURAT TUNA[10], İHSAN PEHLIVAN[11], İSMAIL KOYUNCU[12] AND MOHD ASRUL HERY IBRAHIM[13]

[1]School of Electrical and Communication Engineering, Vel Tech University, Avadi, Chennai-600062, Tamil Nadu, India (e-mail: sundar@veltech.edu.in)
[2]Department of Mechanical Engineering, Universitas Muhammadiyah Tasikmalaya, Tasikmalaya, Jawa Barat 46196, Indonesia (e-mail: acengs@umtas.ac.id)
[3]Center of Excellence in Cybersecurity, Quantum Information Processing, and Artificial Intelligence, Menoufia University, 32511, Egypt (e-mail: bassimeldeeb@gmail.com)
[4]Mathematics Department, Computer Science Laboratory, Faculty of Science, Menoufia University, Shebin El-Koom 32511, Egypt (e-mail: a.rahiem@gmail.com)
[5]Department of Electronics, INAOE, Tonantzintla, Puebla 72840, Mexico (e-mail: etelo@inaoep.mx)
[6]Department of Electronics, INAOE, Tonantzintla, Puebla 72840, Mexico (e-mail: ing.omargufe@gmail.com)
[7]Faculty of Informatics and Computing, Universiti Sultan Zainal Abidin, Kuala Terengganu 21300, Malaysia (e-mail: must@unisza.edu.my)
[8]Faculty of Informatics and Computing, Universiti Sultan Zainal Abidin, Kuala Terengganu 21300, Malaysia (e-mail: mafendee@unisza.edu.my)
[9]Department of Mechatronics Engineering, Technology Faculty, Afyon Kocatepe University, Afyon,Turkey (e-mail: muratalcin@aku.edu.tr)
[10]Department of Electric, Technical Sciences Vocational School, Kirklareli University, Kirklareli, Turkey (e-mail: murat.tuna@klu.edu.tr)
[11]Department of Electrical and Electronics Engineering, Technology Faculty, Sakarya Applied Sciences University, Sakarya, Turkey (e-mail: ipehlivan@sakarya.edu.tr)
[12]Department of Electrical and Electronics Engineering, Technology Faculty, Afyon Kocatepe University, Afyon, Turkey (e-mail: ismailkoyuncu@aku.edu.tr)
[13] Faculty of Entrepreneurship and Business, Universiti Malaysia Kelantan 16100 Kota Bharu Kelantan, Malaysia (e-mail: hery.i@umk.edu.my)

Corresponding author: Mohamad Afendee Mohamed (e-mail: mafendee@unisza.edu.my).

This project is funded by the Center for Research Excellence, Incubation Management Center, Universiti Sultan Zainal Abidin, Malaysia

ABSTRACT In this work, we devise a new 5-D hyperchaotic dynamo system by adding two feedback controllers to the Rikitake 2-disk dynamo system (1958). We show that the new 5-D hyperchaotic system does not possess any equilibrium point and deduce that the new 5-D system has a hidden hyperchaotic attractor. Using Multisim, we develop an electronic circuit design of the new 5-D hyperchaotic dynamo system for practical applications. We also exhibit the implementation of the new 5-D hyperchaotic dynamo system by using a field-programmable gate array (FPGA), which requires adders, subtractors and multipliers. The hardware resources are given for the application of three numerical methods, all of them providing results in good agreement with MATLAB simulations. As an application, we devise a dual core high speed hybrid true random number generator (TRNG) using Ring and Heun algorithm based on the new 5-D hyperchaotic oscillator on FPGA. Based on the hyperchaotic features of the proposed 5-D hyperchaotic dynamo system, we suggest a new encryption approach for colour images. Simulation outcomes of the presented encryption approach confirm that our chaotic system has good cryptographic properties and its usability in different cryptographic purposes.

INDEX TERMS Hyperchaos, hyperchaotic systems, hidden attractors, multi-stability, circuit design,FPGA, TRNG, data protection, image encryption.

This article has been accepted for publication in a future issue of this journal, but has not been fully edited. Content may change prior to final publication. Citation information: DOI 10.1109/ACCESS.2021.3085483, IEEE Access

I. INTRODUCTION

HYPERCHAOTIC SYSTEMS have many applications in science and engineering due to their high complexity arising from the existence of two or more positive Lyapunov exponents [1]. Singh et al. (2020) discussed a secure communication application using a new hyperchaotic system with a stable equilibrium [2]. An et al. (2021) designed a new simple hyperchaotic system with dual memristors and applied it for a secure communication system [3]. Using a hyperchaotic Lorenz system, Ouannas et al. (2021) suggested a new secure communication system, which is obtained by combining chaotic modulation, recursive encryption and chaotic masking [4]. Sahin et al. (2020) proposed a memristor based 4-D hyperchaotic circuit and implemented it for communication systems on FPGA platform [5]. Yang et al. (2020) suggested an image compression and encryption algorithm based on fractional-order memristive hyperchaotic system and back propagation neural network [6]. Ahmad et al. (2021) proposed an image cryptosystem based on hyperchaotic system [7]. Using a new hyperchaotic Chen system, Zhong and Pan (2020) proposed a new image encryption algorithm [8]. Using a new hidden memristive hyperchaotic attractor, Vaidyanathan et al. (2019) suggested a new voice encryption scheme [9]. Fang and Sun (2018) devised a new image steganography scheme based on hyperchaotic map and DNA sequence [10].

Modelling and engineering applications of 5-D hyperchaotic systems are important research problems in the hyperchaos literature ([11]–[15]). Yang et al. (2019) reported a 5-D hyperchaotic system with self-excited and two types of hidden hyperchaotic attractors [11]. Singh et al. (2018) modelled a 5-D multistable hyperchaotic system with a stable equilibrium point and transient chaotic behavior [12]. Zhang et al. (2018) reported a 5-D hyperchaotic system of Lorenz type and discussed its dynamic properties [13]. Wang et al. (2018) used the technique of flux-controlled memristor for developing a 5D system with hyperchaos characteristics and gave a MultiSim electronic simulation for the new system [14]. Koyuncu et al. implemented a 5-D hyperchaotic Lorenz system on FPGA using Heun algorithm to improve the chaos-based embedded engineering applications [15].

Recently, chaotic attractors are classified under two categories, viz. (A) self-excited attractors, and (B) hidden attractors ([16], [17]). A chaotic attractor is called self-excited when its basin of attraction overlaps with neighborhood of an equilibrium point of the system. Chaotic attractors, which are not self-excited, are called hidden attractors.

In this research work, we obtain a new 5-D hyperchaotic system by adding two feedback controls to the Rikitake 2-disk dynamo system [18]. We show that the new 5-D hyperchaotic system does not contain any equilibrium point. We deduce that the new 5-D system belongs to the class of hyperchaotic systems exhibiting hidden attractors. We also describe the multi-stability property of the new 5-D hyperchaotic system.

Circuit designs of chaotic and hyperchaotic systems enable their practical applications ([19]–[22]). In this work, we have used MultiSim for electronic circuit design of the proposed 5-D hyperchaotic system with no equilibrium point.

Chaotic and hyperchaotic oscillators have been active topics for research during the last years due to its usefulness in the development of chaotic secure communication systems and other applications that have been implemented using either analog or digital electronics, as already shown in [23]. In recent years, great efforts have been carried out on the development of chaos-based true random number generator (TRNG) structures due to the features ([24]–[26]) including noise-like properties and hiding the information signal of chaotic oscillators ([27]–[29]). Random number generators have been used in many areas including cryptography, applications using the Monte-Carlo method, computer simulations and modeling and numerical analysis applications ([30]–[33]).

Information security plays an important task in our everyday lives ([34], [35]). Images are the most common data presentation model. The data represented by images can be protected by using one of the image data hiding techniques or using one of the image encryption models ([36]–[38]). Due to the chaotic features of our chaotic map, we propose a new encryption scheme for colour images. The outcome of our chaotic system generates five sequences. In the presented encryption scheme, the first generated sequence is utilized for shuffling the elements of each row and the second sequence is utilized for shuffling the elements of each column, while the last three sequences are utilized in substitution process. Then the initial conditions of our chaotic system are updated according to some information gained from the substituted image and utilizing the generated first three sequences for substituting the substituted image. Simulation outcomes of the presented encryption approach confirm that our chaotic system has good cryptographic properties and its usability in different cryptographic purposes.

II. A NEW 5-D HYPERCHAOTIC SYSTEM WITH NO EQUILIBRIUM POINT

The Rikitake dynamo model of geomagnetic reversals [18] is described by the following 3-D dynamics:

$$\begin{cases} \dot{y}_1 &= -ay_1 + y_2y_3 \\ \dot{y}_2 &= -ay_2 + (y_3 - b)y_1 \\ \dot{y}_3 &= 1 - y_1y_2 \end{cases} \tag{1}$$

In the 3-D Rikitake dynamo model (1), y_1 and y_2 represent the electric currents, while y_3 represents the angular velocity. For $(a, b) = (1, 1)$ and $Y(0) = (0.3, 0.1, 0.2)$, the Lyapunov characteristic exponents of the Rikitake dynamo model (1) are numerically determined for $T = 1E5$ seconds using MATLAB as $\mu_1 = 0.1284$, $\mu_2 = 0$ and $\mu_3 = -2.1284$.

Vaidyanathan et al. [39] obtained a new 4-D hyperchaotic dynamo system by means of adding a feedback control y_4

This article has been accepted for publication in a future issue of this journal, but has not been fully edited. Content may change prior to final publication. Citation information: DOI 10.1109/ACCESS.2021.3085483, IEEE Access

to the Rikitake dynamo model (1), which can be stated as follows:

$$\begin{cases} \dot{y}_1 &= -ay_1 + y_2y_3 - dy_4 \\ \dot{y}_2 &= -ay_2 + (y_3 - b)y_1 - dy_4 \\ \dot{y}_3 &= 1 - y_1y_2 \\ \dot{y}_4 &= cy_1 \end{cases} \tag{2}$$

It was established in [39] that the 4-D dynamo system (2) possesses a hyperchaotic attractor for the parameter values $(a, b, c, d) = (1, 1, 5, 6)$ and $Y(0) = (0.3, 0.1, 0.2, 0.3)$ with the Lyapunov characteristic exponents obtained for $T = 1E5$ seconds using MATLAB as $\mu_1 = 0.1664$, $\mu_2 = 0.0335$, $\mu_3 = 0$ and $\mu_4 = -2.1991$.

In this work, we announce a new 5-D dynamical system by means of adding a new feedback control y_5 into the 4-D Vaidyanathan dynamo system (2). Our new dynamical system is described as follows:

$$\begin{cases} \dot{y}_1 &= -ay_1 + y_2y_3 - dy_4 - qy_5 \\ \dot{y}_2 &= -ay_2 + (y_3 - b)y_1 - dy_4 - qy_5 \\ \dot{y}_3 &= 1 - y_1y_2 \\ \dot{y}_4 &= cy_1 \\ \dot{y}_5 &= py_1 \end{cases} \tag{3}$$

We will establish that the 5-D system (3) has a hyperchaotic attractor with three positive Lyapunov exponent values for the values of the constant parameters chosen as

$$a = 1,\ b = 1,\ c = 5,\ d = 6,\ p = 6,\ q = 8 \tag{4}$$

The Lyapunov exponents of the 5-D system (3) for the constant parameters as in (4) and $Y(0) = (0.3, 0.1, 0.2, 0.3, 0.2)$ were calculated for $T = 1E5$ in MATLAB as follows:

$$\begin{cases} \mu_1 &= 0.2074 \\ \mu_2 &= 0.0132 \\ \mu_3 &= 0.0050 \\ \mu_4 &= 0 \\ \mu_5 &= -2.2257 \end{cases} \tag{5}$$

We note that for the 5-D system (3), $\mu_1 = 0.2074$, and for the 4-D system (2), $\mu_1 = 0.1664$. Also, the 5-D system (3) has 3 positive Lyapunov exponents, while the 4-D system (2) has 2 positive Lyapunov exponents.

Next, we suppose that $(a, b, c, d, p, q) = (1, 1, 5, 6, 6, 8)$ (hyperchaotic case) and calculate the equilibrium points of the 5-D system (3) by means of solving the following system of equations:

$$-ay_1 + y_2y_3 - dy_4 - qy_5 = 0 \tag{6a}$$

$$-ay_2 + (y_3 - b)y_1 - dy_4 - qy_5 = 0 \tag{6b}$$

$$1 - y_1y_2 = 0 \tag{6c}$$

$$cy_1 = 0 \tag{6d}$$

$$py_1 = 0 \tag{6e}$$

Since $c > 0$, we deduce from (6d) that $y_1 = 0$. This contradicts (6c). Hence, we conclude that the system (3) has no equilibrium point. Hence, it is implied that the hyperchaotic system (3) has a hidden hyperchaotic attractor.

We also observe that the 5-D system (3) has rotation symmetry about the y_3-axis since the system dynamics is invariant under the changes of coordinates

$$(y_1, y_2, y_3, y_4, y_5) \mapsto (-y_1, -y_2, y_3, -y_4, -y_5) \tag{7}$$

for all values of the system parameters a, b, c, d and p.

The signal plots of the 5-D hyperchaotic system (3) for the constant parameters $(a, b, c, d, p, q) = (1, 1, 5, 6, 6, 8)$ (hyperchaotic case) and the initial state $Y(0) = (0.3, 0.1, 0.2, 0.3, 0.2)$ are simulated in Figure 1, while the hyperchaotic time series of the 5-D system (3) is simulated in Figure 2.

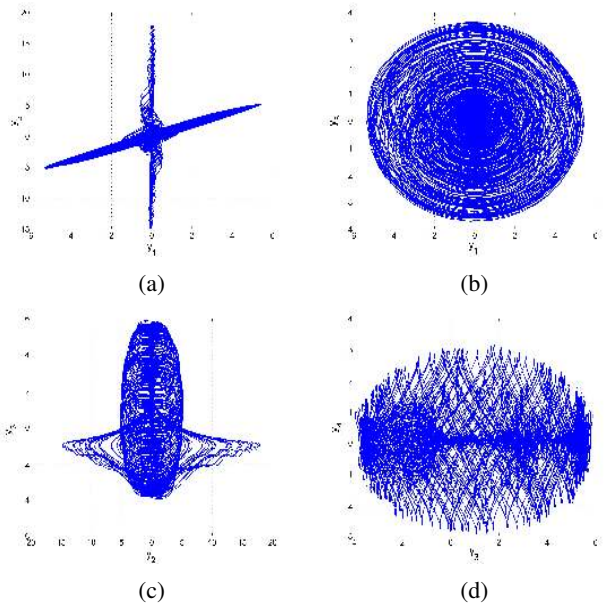

FIGURE 1: 2-D plots of the 5-D hyperchaotic system (3) for $(a, b, c, d, p, q) = (1, 1, 5, 6, 6, 8)$ and the initial state $Y(0) = (0.3, 0.1, 0.2, 0.3, 0.2)$: (a) (y_1, y_2) plane, (b) (y_1, y_5) plane, (c) (y_2, y_3) plane and (d) (y_3, y_4) plane.

Coexistence of multiple attractors means that under fixed nonlinear dynamic system parameters, the system has different types of attractors, each of which is excited and generated from the initial state corresponding to a different basin of attraction, showing the bistability or multistability of a nonlinear dynamic system ([40], [41]). Bistability or multistability is a peculiar phenomenon, that is, more than one asymptotically stable states coexist in a nonlinear dynamic system with determined parameters, which reflects the sensitivity of system dynamics to initial conditions.

Since the 5-D dynamo system (3) has rotation symmetry about the y_3 axis, it can generate coexisting attractors that are symmetric about the y_3 axis. When the parameters are taken as $a = 1$, $b = 1$, $c = 5$, $p = 1$ and $q = 1$,

This article has been accepted for publication in a future issue of this journal, but has not been fully edited. Content may change prior to final publication. Citation information: DOI 10.1109/ACCESS.2021.3085483, IEEE Access

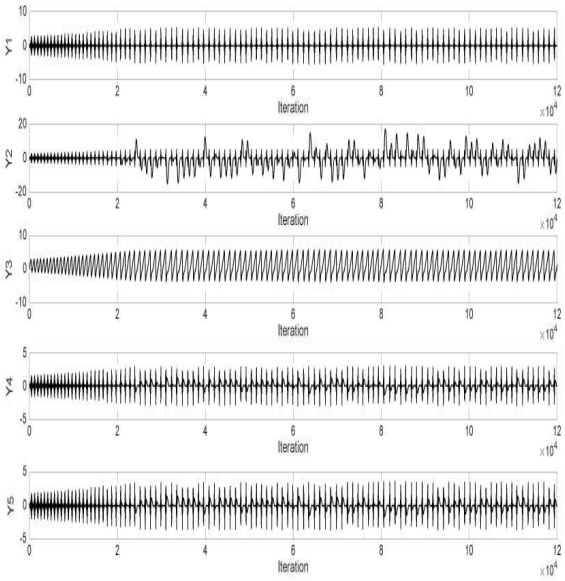

FIGURE 2: Hyperchaotic time series of the new 5-D hyperchaotic dynamo system (3).

and the initial state are set to $Y_0 = (2, 0.1, 0.2, 0.3, 0.2)$ and $Z_0 = (-2, -0.1, 0.2, -0.3, -0.2)$, the coexisting bifurcation diagram of the state variable y_5 with respect to the control parameter d in the range of $[0, 10]$ and the corresponding Lyapunov exponents with the initial state $Y_0 = (2, 0.1, 0.2, 0.3, 0.2)$ are illustrated in Figures 3 (a) and (b), respectively. In Figure 3, the blue orbit starts with the initial state Y_0 and the red orbit starts with the initial state Z_0. From Figure 3, it is easy to observe that the 5-D dynamo system (3) is in periodic state at first and finally drops into non-period (chaos or hyperchaos) except for three periodic windows. Besides, there exist coexisting attractors (coexisting periodic attractors, coexisting chaotic attractors and coexisting hyperchaotic attractors) in the whole region. Some typical phase portraits of different types of coexisting attractors of the 5-D system (3) are displayed in Figure 4.

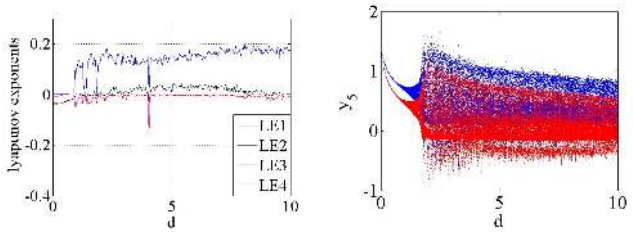

(a) (b)

FIGURE 3: Coexisting bifurcation of the 5-D system (3) with respect to d for $a = 1$, $b = 1$, $c = 5$, $p = 1$, $q = 1$, and the initial condition $Y_0 = (2, 0.1, 0.2, 0.3, 0.2)$: (a) coexisting bifurcation diagram and (b) the Lyapunov exponents.

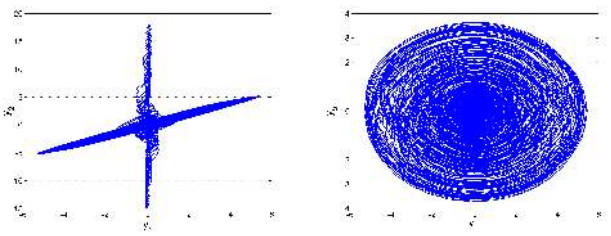

(a) (b)

FIGURE 4: Coexisting attractors of the 5-D dynamo system (3) with respect to d for $a = 1$, $b = 1$, $c = 5$, $p = 1$, $q = 1$, and the initial states $Y_0 = (2, 0.1, 0.2, 0.3, 0.2)$ and $Z_0 = (-2, -0.1, 0.2, -0.3, -0.2)$: (a) coexisting chaotic attractors with $d = 1.2$, (b) coexisting hyperchaotic attractors with $d = 6$.

III. CIRCUIT DESIGN OF THE 5-D HYPERCHAOTIC DYNAMO SYSTEM

In this section, an electronic circuit design of the 5-D hyperchaotic dynamo system (3) is modelled via Multisim software, version 13.0. The electronic circuit includes seven operational amplifiers, three multipliers, five capacitors and 17 resistors. It is noted that five operational amplifiers (U1A, U3A, U4A, U5A, U7A) are configured as integrators while two operational amplifiers U2A, U6A are configured as inverting amplifier.

For the circuit implementation, the new 5-D hyperchaotic dynamo system (3) has to be rescaled by using $Y_1 = 2y_1$, $Y_2 = 2y_2$, $Y_3 = 2y_3$, $Y_4 = 2y_4$ and $Y_5 = 2y_5$.

After rescaling the state variables in (3), we obtain the following new 5-D hyperchaotic system:

$$\begin{cases} \dot{Y}_1 &= -aY_1 + \frac{1}{2}Y_2Y_3 - dY_4 - qY_5 \\ \dot{Y}_2 &= -aY_2 + \frac{1}{2}Y_1Y_3 - bY_1 - dY_4 - qY_5 \\ \dot{Y}_3 &= 2 - \frac{1}{2}Y_1Y_2 \\ \dot{Y}_4 &= cY_1 \\ \dot{Y}_5 &= pY_1 \end{cases} \tag{8}$$

Upon applying Kirchhoff's electrical circuit laws to the current of Figure 5, the following dynamics for the new 5-D hyperchaotic dynamo system (8) can be derived:

$$\begin{cases} \dot{Y}_1 &= -\frac{1}{C_1R_1}Y_1 + \frac{1}{C_1R_2}Y_2Y_3 - \frac{1}{C_1R_3}Y_4 - \frac{1}{C_1R_4}Y_5 \\ \dot{Y}_2 &= -\frac{1}{C_2R_5}Y_2 + \frac{1}{C_2R_6}Y_1Y_3 - \frac{1}{C_2R_7}Y_1 - \frac{1}{C_2R_8}Y_4 \\ & \quad -\frac{1}{C_2R_9}Y_5 \\ \dot{Y}_3 &= \frac{1}{C_3R_{10}}V_1 - \frac{1}{C_3R_{11}}Y_1Y_2 \\ \dot{Y}_4 &= \frac{1}{C_4R_{12}}Y_1 \\ \dot{Y}_5 &= \frac{1}{C_5R_{13}}Y_1 \end{cases} \tag{9}$$

Here, Y_1, Y_2, Y_3, Y_4 and Y_5 are the voltages across the capacitors C_1, C_2, C_3, C_4, and C_5, respectively. We choose the values of the circuital elements as $R_1 = R_5 = R_7 = 400$

kΩ, $R_2 = R_6 = R_{11} = 800$ kΩ, $R_3 = R_8 = R_{13} = 66.67$ kΩ, $R_4 = R_9 = 50$ kΩ, $R_{10} = R_{11} = 200$ kΩ, $R_{12} = 80$ kΩ, $R_{14} = R_{15} = R_{16} = R_{17} = 100$ kΩ and $C_1 = C_2 = C_3 = C_4 = C_5 = 1$ nF. Multisim phase portraits of the 5-D hyperchaotic circuit (9) are shown in Figure 6. It is observed that the Multisim outputs in Figure 6 show a good match with the 2-D MATLAB plots of the 5-D hyperchaotic dynamic system (3) shown in Figure 1.

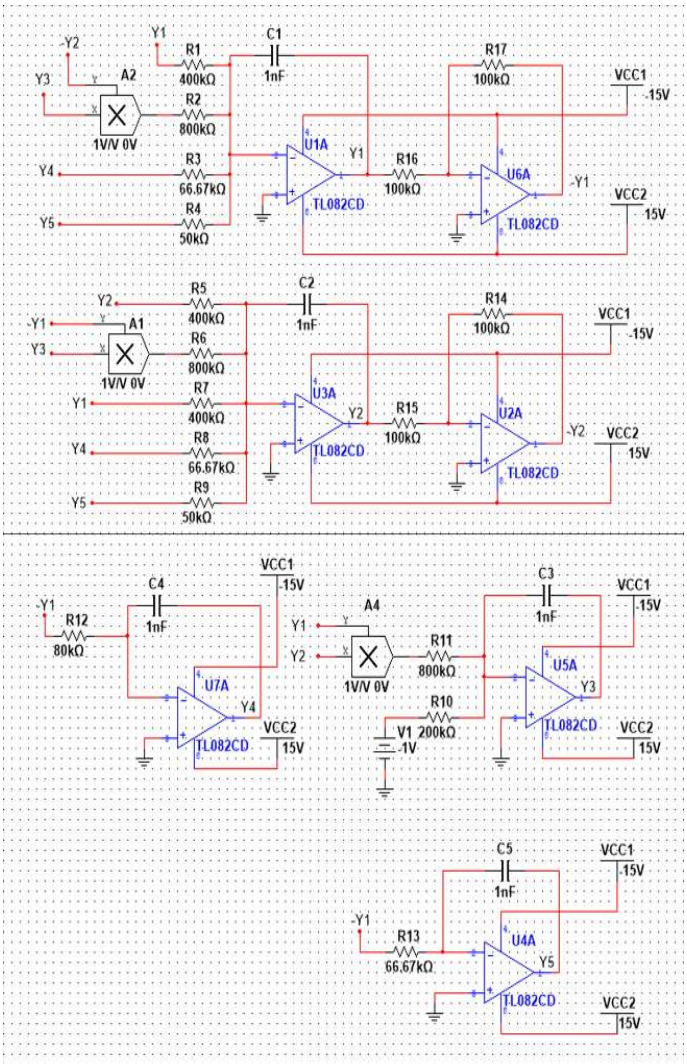

FIGURE 5: Circuit schematic diagram for the 5-D hyperchaotic dynamic system (9)

IV. FPGA DESIGN OF THE NEW CHAOTIC SYSTEM

A field-programmable gate array (FPGA) is an integrated circuit that has the advantage of being reprogrammed/reconfigured in the field after manufacture. Its usefulness for fast prototyping makes it a popular device for low development cost applications, while providing good performance. The FPGA has been applied to implement different chaotic systems, as already shown in ([23], [42]). However, the hardware resources depend on the numerical method that

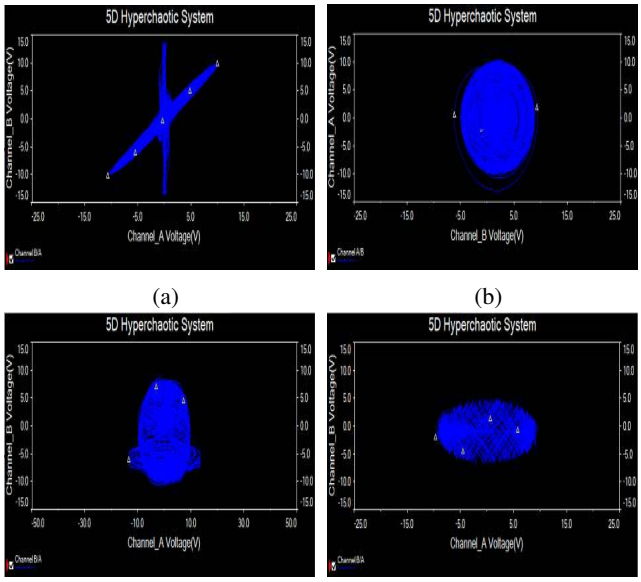

FIGURE 6: 2-D plots of the 5-D hyperchaotic circuit (9) using Multisim circuit simulation: (a) (Y_1, Y_2) plane, (b) (Y_1, Y_5) plane, (c) (Y_2, Y_3) plane and (d) (Y_3, Y_4) plane.

is used to solve the system of equations. In this manner, this section shows the FPGA implementation of the new 5-D hyper-chaotic dynamo system given in (3) by applying three different methods, namely: forward-Euler, trapezoidal and fourth-order Runge-Kutta. Each numerical method provides different accuracy and requires a good estimation of the step-size to diminish numerical errors, as shown in [23]. By applying the Forward Euler method, we get the discrete equations given by (10).

$$\begin{aligned} y_{1_{n+1}} &= y_{1_n} + h[-a y_{1_n} + y_{2_n} y_{3_n}] \\ &\quad + h[-d y_{4_n} - q y_{5_n}] \\ y_{2_{n+1}} &= y_{2_n} + h[-a y_{2_n} + (y_{3_n} - b) y_{1_n}] \\ &\quad + h[-d y_{4_n} - q y_{5_n}] \\ y_{3_{n+1}} &= y_{3_n} + h[1 - y_{1_n} y_{2_n}] \\ y_{4_{n+1}} &= y_{4_n} + h[c y_{1_n}] \\ y_{5_{n+1}} &= y_{5_n} + h[p y_{1_n}] \end{aligned} \tag{10}$$

From the discretized equations given in (10), one can identify the building blocks to be implemented in the FPGA. The high-level description of the interconnected blocks is shown in Fig. 7, where it can be appreciated the use of adders, subtractors and multipliers of two inputs (A,B) and one output (O). An important point is that the multiplication of a state variable by a constant can be realized by designing single-constant multiplier (SCM) blocks, which require low resources compared to a full multiplier. See for example the first and second equations in in (10), the multiplications ay_{1_n}, dy_{4_n}, and qy_{5_n}, as a, d and q are constants, the SCM can be implemented by using adders, subtractors and shifters, thus saving hardware resources and increasing the speed of

This article has been accepted for publication in a future issue of this journal, but has not been fully edited. Content may change prior to final publication. Citation information: DOI 10.1109/ACCESS.2021.3085483, IEEE Access

processing in the FPGA. The SCM is also designed for all the blocks multiplying the step-size (h) in the blocks labeled as Integrator Forward-Euler, and to multiply by c and p in the fourth and fifth equations.

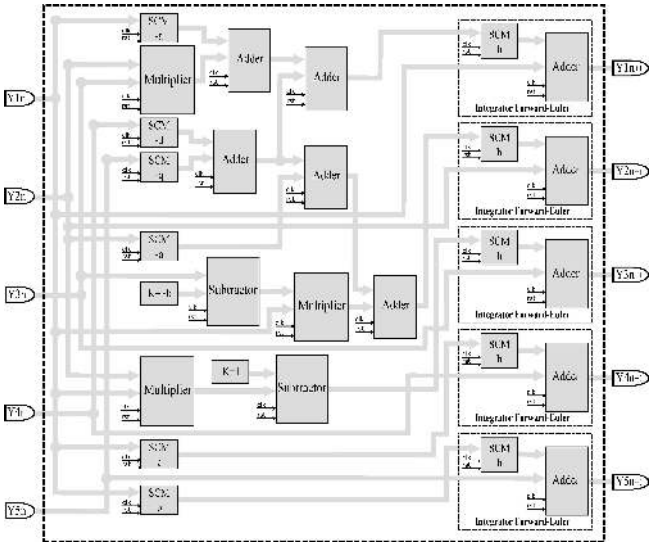

FIGURE 7: Block diagram of the new 5-D hyperchaotic system (3) discretized with Forward-Euler.

The computer arithmetic to process the data in the FPGA implementation depends on the amplitudes of the state variables shown in Fig. 2. From this data, one must take into consideration that the multiplication operations may generate larger values. For example: in the case of the state variables y_1 and y_2, which ranges are near to $[-8, 8]$ and $[-18, 18]$, respectively, one may expect a result of ± 144, and therefore, this value can be represented by using 8 bits. Henceforth, the FPGA implementation can be done by adopting fixed-point notation with the format 9.23 (32 bits), using one for the sign, 8 for the integer part, and 23 for the fractional part in all the blocks shown in Fig. 7.

The discretization and block diagram design for the 5D hyperchaotic system (3) by applying the trapezoidal and Runge-Kutta methods is performed in the same way. By setting $h = 0.01$, Table 1 shows the resources of the implementation of (3) by using the FPGA Cyclone IV EP4CGX150DF31C7 along the synthesizer "Quartus II 13.0". It is worthy mentioning that the row called "Clock cycles by iteration" represents the number of clock cycles that are required to process a new iteration to compute $y_{1_{n+1}}$, $y_{2_{n+1}}$, $y_{3_{n+1}}$, $y_{4_{n+1}}$ and $y_{5_{n+1}}$ with a valid data, and the "Latency" row represents the time to compute a new iteration with a 50 MHz clock signal.

Figures 8, 9, and 10, show the chaotic time series simulated from the VHDL descriptions of the 5D hyperchaotic system (3) by applying the Forward Euler, Trapezoidal and the fourth-order Runge-Kutta methods. It can be noted that the ranges of the discretized state variables are quite similar to the ones obtained by MatLab simulations, as shown in Fig. 2. However, as in the FPGA the computer arithmetic was performed by using 32 bits, then the evolution of the trajectories

TABLE 1: Hardware resources for the implementation of the 5D hyperchaotic system (3) by using the FPGA Cyclone IV EP4CGX150DF31C7, and by applying the Forward-Euler, Trapezoidal and Runge-Kutta methods with $h = 0.01$.

Resources	Forward-Euler	Trapezoidal	Runge-Kutta	Available
[2mm] Logic Elements	1,648	3,493	6,954	149,760
Registers	1112	1340	1554	149,760
9×9 Bit multipliers	36	72	144	720
Max Freq. (MHz)	99.6	98.1	97.3	50
Clock cycles by Iteration	11	21	43	-
Latency (ns)	220	420	860	-

is a little different because there exists a truncation error, but the dynamical characteristics such as Lyapunov exponents values remain the same. One can increase the number of bits to gain more accuracy.

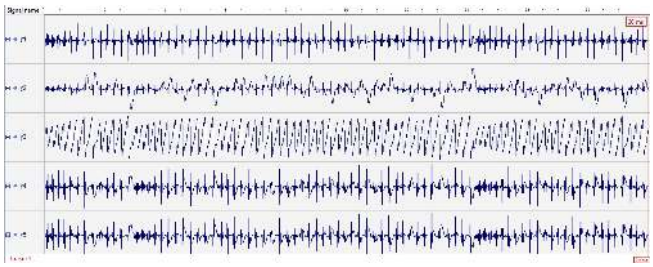

FIGURE 8: Hyperchaotic time series of the 5D system (3) from the FPGA implementation by applying the Forward-Euler method.

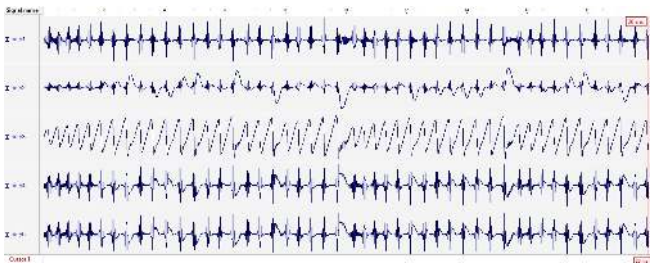

FIGURE 9: Hyperchaotic time series of the 5D system (3) from the FPGA implementation by applying the Trapezoidal method.

V. THE NEW 5-D HYPERCHAOTIC DYNAMO SYSTEM AND RING BASED DUAL CORE TRNG

Chaotic and hyperchaotic systems are complex and irregular looking, sensitive to initial conditions, and they exist in deterministic nonlinear systems that change over time.

This article has been accepted for publication in a future issue of this journal, but has not been fully edited. Content may change prior to final publication. Citation information: DOI 10.1109/ACCESS.2021.3085483, IEEE Access

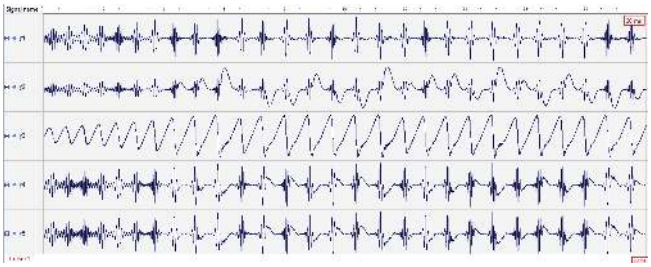

FIGURE 10: Hyperchaotic time series of the 5D system (3) from the FPGA implementation applying the fourth-order Runge-Kutta method.

Important studies have been carried out in scientific and industrial fields for the research and implementation of these systems. In recent years, great efforts have been carried out on the development of chaos-based TRNG structures due to the features ([24]–[26]) including noise-like properties and hiding the information signal of chaotic oscillators ([27]–[29]). Random number generators have been used in many areas including cryptography, applications using the Monte-Carlo method, computer simulations and modeling and numerical analysis applications ([30]–[33]). In this study, the designed Heun based discrete mathematical model of a new 5-D hyperchaotic dynamo system is given by the system of equations (11).

$$
\begin{aligned}
y_1^0(k+1) = \;& y_1(k) + [-ay_1(k)]\Delta h \\
& + [y_2(k)y_3(k) - dy_4(k) - qy_5(k)]\Delta h \\
y_1(k+1) = \;& y_1(k) + \tfrac{[-ay_1(k)+y_2(k)y_3(k)]}{2}\Delta h \\
& + \tfrac{[-dy_4(k)-qy_5(k)]+y_1^0(k+1)}{2}\Delta h \\
y_2^0(k+1) = \;& y_2(k) + [-ay_2(k) + (y_3(k) - b)y_1(k)]\Delta h \\
& + [-dy_4(k) - qy_5(k)]\Delta h \\
y_2(k+1) = \;& y_2(k) + \tfrac{[-ay_2(k)+(y_3(k)-b)y_1(k)]}{2}\Delta h \\
& + \tfrac{[-dy_4(k)-qy_5(k)]+y_2^0(k+1)}{2}\Delta h \\
y_3^0(k+1) = \;& y_3(k) + [1 - y_1(k)y_2(k)]\Delta h \\
y_3(k+1) = \;& y_3(k) + \tfrac{[1-y_1(k)y_2(k)]+y_3^0(k+1)}{2}\Delta h \\
y_4^0(k+1) = \;& y_4(k) + [cy_1(k)]\Delta h \\
y_4(k+1) = \;& y_4(k) + \tfrac{[cy_1(k)]+y_4^0(k+1)}{2} \\
y_5^0(k+1) = \;& y_5(k) + [py_1(k)]\Delta h \\
y_5(k+1) = \;& y_5(k) + \tfrac{[py_1(k)]+y_5^0(k+1)}{2}\Delta h
\end{aligned}
\tag{11}
$$

From the mathematical model (11), it can be seen that the Heun algorithm is a two-step algorithm. In the first stage, $y_1^0(k+1)$ value has been calculated by using the values of $y_i(k), (i = 1, 2, 3, 4, 5)$. In the second stage, using the values of $y_1^0(k+1)$ and $y_i(k)$, the value of $y_1(k+1)$ is calculated, where Δh denotes the step-size. Similarly, $y_2(k+1)$, $y_3(k+1)$, $y_4(k+1)$ and $y_5(k+1)$ are calculated in (11).

The dual entropy core high speed TRNG unit designed using the 5-D new hyper chaotic oscillator and ring oscillator structures using Heun algorithm on FPGA is presented in Figure 11. The random number sequences, that have high operating frequency and bit generation rate obtained from the proposed structure; will be able to be used in cryptography and secure communication areas where fast, secure and intensive processes needed. The designed chaotic TRNG unit was synthesized for the XC7VX485T-2-FFG1761 chip of the Virtex-7 VC707 family produced by Xilinx company. The statistics of the parameters of FPGA chip resource usage and clock speed of the units have been examined. The data processing time of TRNG units was obtained using the Xilinx ISE Design Tools 14.2 simulation program.

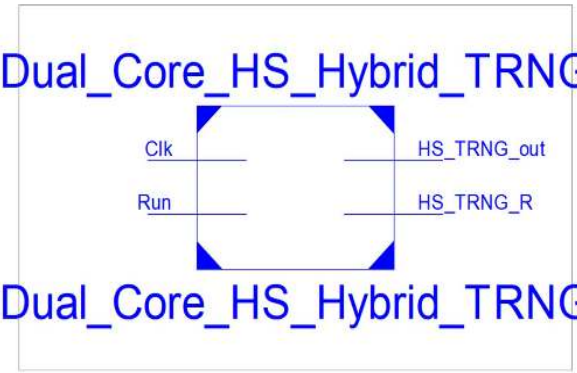

FIGURE 11: The top-level block diagram of the dual core high speed hybrid TRNG using Ring and Heun algorithm based on the new 5D hyperchaotic oscillator on FPGA.

Figure 12 shows the block diagram of the FPGA based dual core TRNG unit. TRNG unit, designed by Heun-based on FPGA, consists of 5 parts: x5mux, New_5D_HCO_HEUN oscillator, Quantization unit, Ring oscillator and Art unit. In design, the x5mux unit is basically a multiplexer (MUX) structure developed for the control of the starting signals required by the New_5D_HCO_HEUN unit, which has 5 dependent variables. The system has 5 initial condition values (x0, y0, z0, w0 and v0). Also, as soon as the New_5D_HCO_HEUN unit results (x, y, z, w and v), these results are entered as the initial value for the next iteration of the New_5D_HCO_HEUN unit. As a result, unlike standard MUX structures, there are 10 32-bit inputs in total with 2 having 5 signal inputs. If the New_5D_HCO_HEUN unit did not generate its initial value, the x5mux unit sends its initial values to the New_5D_HCO_HEUN unit. If the New_5D_HCO_HEUN unit produced its first value, the x5mux unit sends the values generated by the New_5D_HCO_HEUN unit as the initial values to the input of this unit. The new_5D_HCO_HEUN

This article has been accepted for publication in a future issue of this journal, but has not been fully edited. Content may change prior to final publication. Citation information: DOI 10.1109/ACCESS.2021.3085483, IEEE Access

unit is designed for the Heun algorithm based operation of the new 5-D hyperchaotic oscillator presented in this work.

In Figure 13, the third level block diagram of dual core high speed hybrid TRNG using Ring and Heun algorithm based on the new 5-D hyperchaotic oscillator on FPGA is presented. Here, the structure of the New_5D_HCO_HEUN unit is given in more detail. All the multiplier, adder and subtractor units used in these designs were created using the IP Core generator developed with Xilinx ISE Design Tools. The new_5D_HCO_Heun oscillator produces the chaotic signals that TRNG needs and transmits these values to 32-bit X_out, Y_out, Z_out, W_out and V_out signals. When the chaotic oscillator produces an output, the 1-bit TRNG_Ready signal becomes '1' and sends the values generated by the new 5-D hyperchaotic oscillator to the Quantization unit. The quantization process was performed by taking the last 23 bits of the fractional part of the 32-bit number in the floating-point number standard produced by each floating-point-based chaotic oscillator unit. The RN signal, obtained from this unit's output, is the signals by which random numbers are carried. The sh signal indicates that random signals are received from the unit output. These two signals are transferred to the ART unit. The post processing is applied for the signals obtained in the ART unit.

In this research work, XOR operation was applied as the post processing and the results were sent to the output of the system. The random numbers generated by the ring oscillator and the random numbers generated by the 5-D new hyperchaotic oscillator-based TRNG unit are subjected to XOR process in the ART_PROCESSING unit. In TRNG structures subjected to the XOR process presented in the literature, the bit production rate is reduced by half as a result of the XOR process. However, unlike the studies presented in the literature, since the random numbers have been generated by using the outputs of 2 different sources in XOR process, there is no decrease in throughput of the presented dual core high speed hybrid TRNG using Ring and Heun algorithm based new 5-D hyperchaotic oscillator on FPGA design.

The dual core high speed hybrid TRNG using Ring and Heun algorithm based new 5-D hyperchaotic oscillator on FPGA has been synthesised for target device XC7VX485T-2-FFG1761 chip. Then, the chip statistics have been obtained. As shown in Table 2, after the Place-Route processes, the maximum clock frequency of the dual core high speed hybrid TRNG using Ring and Heun algorithm based new 5-D hyperchaotic oscillator on FPGA reaches 416.194 MHz. In other words, the minimum clock period of the design was obtained as 2.403 ns.

Figure 14 gives the testbench results whose code is written in VHDL for dual core high speed hybrid TRNG using Ring and Heun algorithm based on 5-D new Hyper chaotic oscillator on FPGA unit. As can be seen in testbench, dual core high speed hybrid TRNG using Ring and Heun algorithm based 5-D new Hyper chaotic oscillator on FPGA unit produces results in every clock pulse. For this reason, the dual core high speed hybrid TRNG using Ring and Heun algorithm based on 5-D new Hyper chaotic oscillator unit can generate 416 Mbit random numbers in 1 second on the Virtex-7 VC707 Evaluation Platform.

The randomness and statistical properties of random number generators developed for use in cryptological applications should be examined and tested. Although, the randomness of the output of the number generators cannot be proven mathematically, it can be said whether the number sequences are random or not by applying valid statistical tests. These tests provide information on whether the output of the generator meets what is expected from a true random sequence. Also, the results of the tests can be commented on the quality of the RNG. To state that a series of numbers is random, it must pass all tests. The sequence cannot be considered random even if only one test fails [31], [32]. It is seen in Table 3 that the number sequences obtained from the proposed FPGA-based TRNG are successful in all tests of the international NIST 800-22.

VI. IMAGE ENCRYPTION USING THE NEW 5-D HYPERCHAOTIC DYNAMO SYSTEM

Based on the chaotic features of the proposed chaotic map, we suggest a new encryption approach for colour images. The presented encryption scheme requires adjustment for the presented chaotic map as presented in (12).

$$\begin{cases} \dot{y}_1 = (-ay_1 + y_2y_3 - dy_4 - qy_5)\, mod1 \\ \dot{y}_2 = (-ay_2 + (y_3 - b)y_1 - dy_4 - qy_5)\, mod1 \\ \dot{y}_3 = (1 - y_1y_2)\, mod1 \\ \dot{y}_4 = (cy_1)\, mod1 \\ \dot{y}_5 = (py_1)\, mod1 \end{cases} \tag{12}$$

The outcome of the chaotic system (12) generates five sequences. In the presented encryption scheme, the first generated sequence of the system (12) is utilized for shuffling the elements of each row and the second sequence is utilized for shuffling the elements of each column, while the last three sequences are utilized in substitution process. Then the initial conditions of the system (12) are updated according to the substituted image and utilizing the generated first three sequences for substituting the substituted image. The outlines of ciphering and deciphering methods for the proposed encryption mechanism are provided in Figures 15 and 16, respectively, while the encryption procedure is presented in Algorithm 1.

VII. EXPERIMENTAL OUTCOMES FOR THE ENCRYPTION SCHEME

To validate the presented encryption approach, we utilised a laptop with Intel $\mathrm{Core}^{\mathrm{TM}}$ i5 CPU 2.500 GHz and 6 GB RAM with preinstalled MATLAB R2016b. The utilised dataset are consist of four colour images taken from Kodak dataset [43] labelled as PIm01, PIm02, PIm03, and PIm04 each of dimension 768×512 (see Figure 17). The primary conditions and control parameters employed for operating the new 5-

This article has been accepted for publication in a future issue of this journal, but has not been fully edited. Content may change prior to final publication. Citation information: DOI 10.1109/ACCESS.2021.3085483, IEEE Access

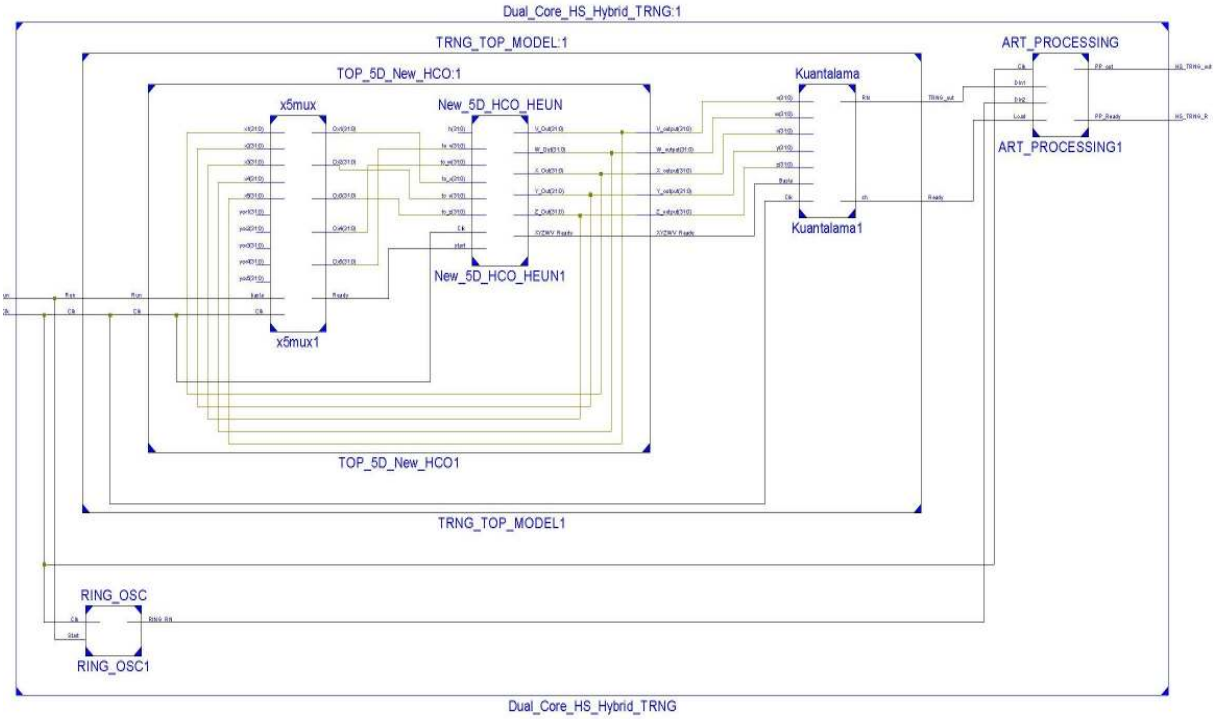

FIGURE 12: The second level block diagram of the dual core high speed hybrid TRNG using Ring and Heun algorithm based on the new 5-D hyperchaotic oscillator on FPGA.

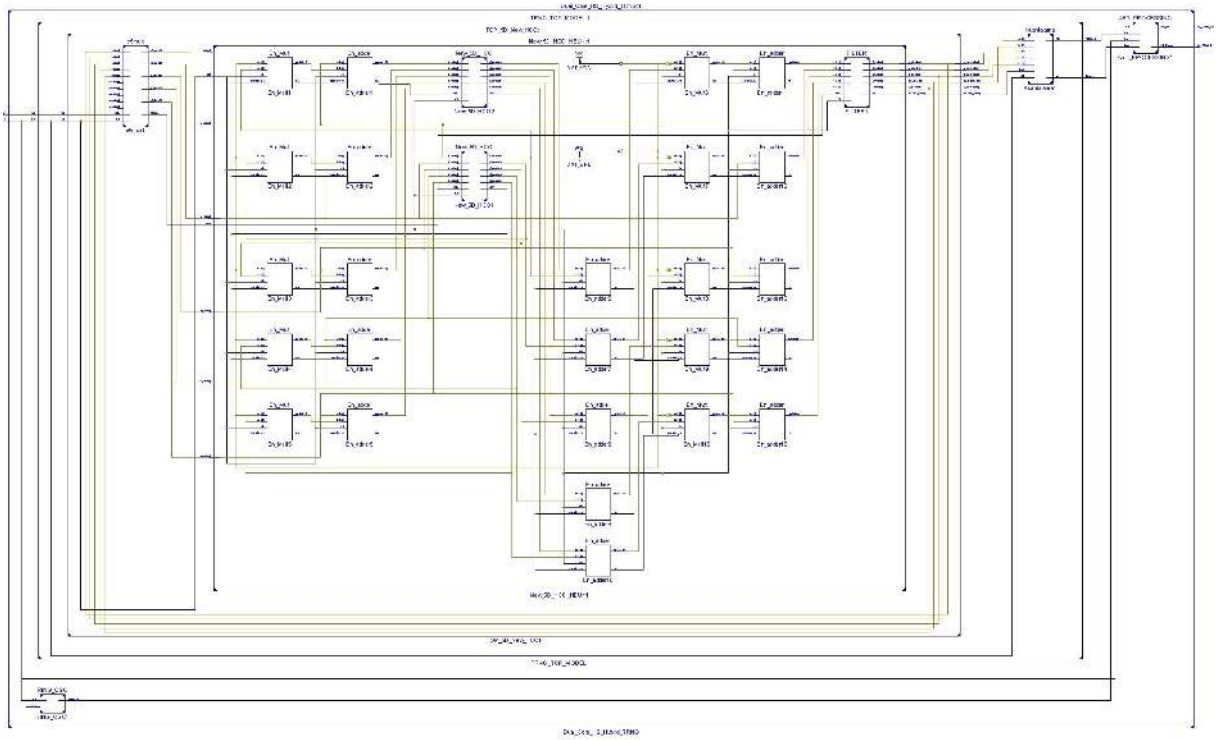

FIGURE 13: The third level block diagram of the dual core high speed hybrid TRNG using Ring and Heun algorithm based on the new 5-D hyperchaotic oscillator on FPGA.

This article has been accepted for publication in a future issue of this journal, but has not been fully edited. Content may change prior to final publication. Citation information: DOI 10.1109/ACCESS.2021.3085483, IEEE Access

TABLE 2: The area utilization report of dual core high speed hybrid TRNG using Ring and Heun algorithm based new 5D hyperchaotic oscillator on Virtex XC7VX485T-2-FFG1761 chip.

Utilization for Virtex-7 VC707 Evaluation Platform	Used	Available	Utilization (%)
Number of Slice Registers	31,702	607,200	5
Number of Slice LUTs	31,708	303,600	10
Number of Fully Used LUT-Flip Flop Pairs	25,342	38,061	66
Number of Inputs / Outputs	4	700	1
Number of BUFG / BUFGCTRLs	1	32	3

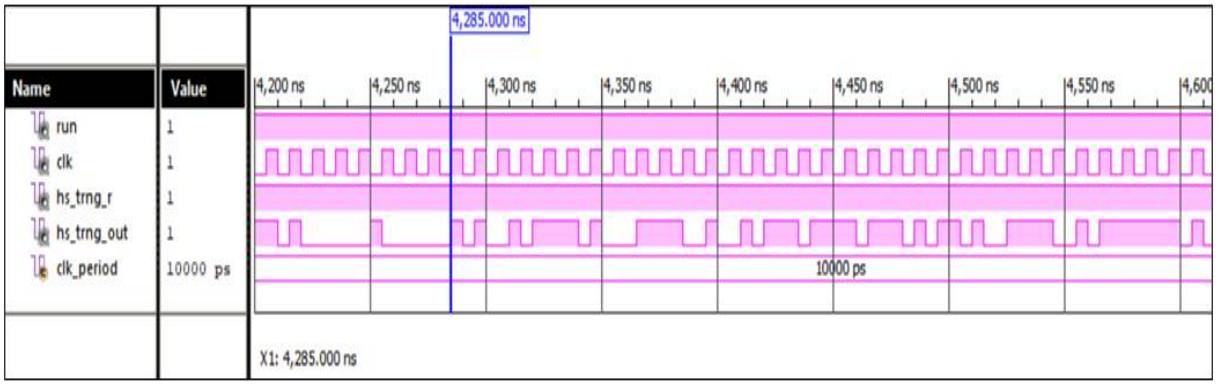

FIGURE 14: The timing diagram results of dual core high speed hybrid TRNG using Ring and Heun algorithm based on the new 5-D hyperchaotic oscillator on FPGA obtained from Xilinx ISE Simulator.

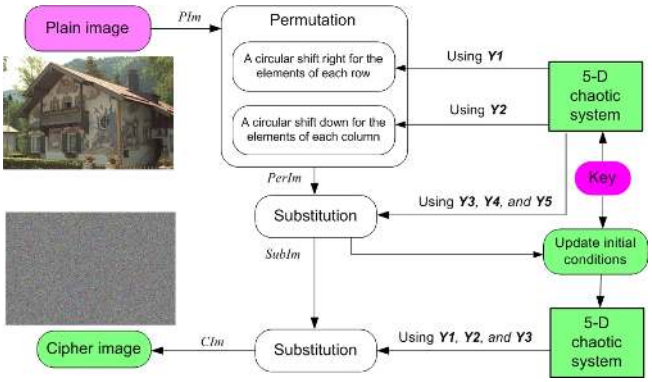

FIGURE 15: Outlines of the ciphering process for the proposed encryption approach.

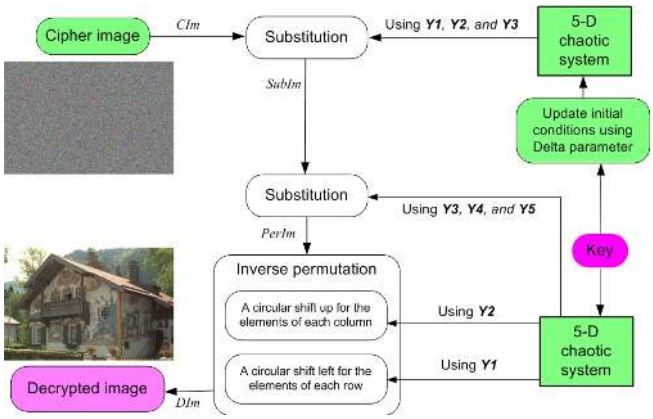

FIGURE 16: Outlines of the deciphering process for the proposed encryption approach.

D chaotic system are defined as $y1_0$=0.3, $y2_0$=0.1, $y3_0$=0.2, $y4_0$=0.3, $y5_0$=0.2, a=1, b=1, c=5, d=6, p=6, and q=8.

A. CORRELATION ANALYSIS

Correlation coefficient of neighbouring pixels C_{pc} is a measure used to assessment the meaningful of an image which normal images have C_{pc} value near to 1 in every direction while in cipher images with a well-designed encryption scheme should near to 0 ([44], [45]). To calculate the outcomes of C_{pc} in every direction of the cipher and plain images, we picked randomly 10^4 pairs of neighbouring pixels in per direction.

$$C_{pc} = \frac{\sum_{i=1}^{N} (p_i - \bar{p})(c_i - \bar{c})}{\sqrt{\sum_{i=1}^{N} (p_i - \bar{p})^2 \sum_{i=1}^{N} (c_i - \bar{c})^2}} \quad (13)$$

where *N* indicates to the entire number of adjacent pixel pairs in any direction and c_i, p_i are points to the values of neighbouring pixels. Table 4 shows the results of C_{pc} for cipher images and their corresponding original ones, which the values of cipher images are very close to 0. Furthermore, Figures 18, 19, and 20 display the distribution of correlations in each

TABLE 3: The NIST test results of dual core high speed hybrid TRNG using Ring and Heun algorithm based on the new 5-D hyperchaotic oscillator on FPGA.

NIST 800-22 Statistical Tests	P-value	Result
Frequency Test	0.18683	Successful
Block Frequency Test	0.82799	Successful
Runs Test	0.69774	Successful
Longest Runs of Ones Test	0.70531	Successful
Binary Matrix Rank Test	0.35665	Successful
Discrete Fourier Transform Test	0.81773	Successful
Non-Overlapping Template Matching Test	0.39259	Successful
Overlapping Template Matching Test	0.26254	Successful
Maurer's Universal Statistical Test	0.31156	Successful
Linear Complexity Test	0.70422	Successful
Serial Test-1	0.77320	Successful
Serial Test-2	0.65583	Successful
Approximate Entropy Test	0.01083	Successful
Cumulative Sums Test	0.11356	Successful
Random Excursions Test (for $x = 1$)	0.91749	Successful
Random Excursions Variant Test (for $x = 2$)	0.96135	Successful

direction for image Im01 and its corresponding ciphered one. From the outcomes stated about correlation coefficient, no beneficial data obtained about the cipher image by analysis C_{pc} values.

B. PIXELS CHANGE RATE

To estimate the sensitivity of tiny changes in the plain image on its corresponding ciphered one, two tools are applied: "Number of Pixels Change Rate" (NPCR) and "Unified Average Changing Intensity" (UACI). The mathematical expressions of NPCR and UACI can be stated in Eq. (14) [46].

$$\begin{aligned} NPCR &= \frac{\sum_{i;j} D(i,j)}{M} \times 100\%, \\ D(i,j) &= \begin{cases} 0 \; if \; C1(i,j) = C2(i,j) \\ 1 \; if \; C1(i,j) \neq C2(i,j) \end{cases} \end{aligned} \tag{14}$$

$$UACI = \frac{1}{M}\left(\sum_{i,j} \frac{|C1(i,j) - C2(i,j)|}{2^N - 1}\right) \times 100\% \tag{15}$$

where C1, C2 are two ciphered images for one plain image with tiny changes, M denotes to the complete number of pixels utilised in the image and N signifies to the number of bits utilised to signify the pixel value. The UACI and NPCR values are stated in Table 5 which all values of NPCR for the experimented dataset are greater than 99.60%. Therefore, the proposed encryption approach is highly sensitive to tiny pixel variations in the plain image.

C. HISTOGRAM TEST

Histogram analysis reflects the frequency distribution of pixel values in the image. A well-designed encryption mechanism must ensure even distribution of various ciphered images to withstand statistical attacks. Figure 21 shows the histograms of Im01 image before and after encryption which histograms of PIm01 image differ from each other, while the diagrams of the CIm01 image are identical with each other. To verify the histogram test for ciphered images we execute chi-square test (χ^2), which can be stated as given in Eq. (16).

$$\chi^2 = \sum_{p}^{g} \frac{(f_p - d)^2}{d} \tag{16}$$

here, g is 255 for 8-bit grey-scale images, f_p points to the frequency of the pixel value p (p=0, 1, 2,..., g), and d is the dimension of the image. On assuming the significant level is α=0.05, then $\chi^2_\alpha(255) = 293.248$. For an image, if the value of χ^2 test is less than $\chi^2_\alpha(255)$, this verify the uniform distribution of the image, otherwise, the image has not uniform distribution [47]. Table 6 displays the outcomes of χ^2 for the experimented dataset, which the values of χ^2 for all plain images are greater than $\chi^2_\alpha(255)$, while the χ^2 values for all ciphered images is less than $\chi^2_\alpha(255)$. Therefore, the provided encryption scheme can resist histogram attacks.

D. INFORMATION ENTROPY ANALYSIS

Global entropy is a statistical test of the distribution for pixel values for per level in an image, which can be expressed

This article has been accepted for publication in a future issue of this journal, but has not been fully edited. Content may change prior to final publication. Citation information: DOI 10.1109/ACCESS.2021.3085483, IEEE Access

Algorithm 1: Ciphering process

Input: Original-image (PIm)
parameter: $y1_0$, $y2_0$, $y3_0$, $y4_0$, $y5_0$, a, b, c, d, p, q
Output: Cipher-image (CIm) and Delta

$[H,\ W,\ L] \leftarrow dimension(PIm)$// Gets the dimensional of the plain image
$[Y1\ \ Y2\ \ Y3\ \ Y4\ \ Y5] \leftarrow new\ 5D\ chaotic\ system(y1_0,\ y2_0,\ y3_0,\ y4_0,\ y5_0,\ a,\ b,\ c,\ d,\ p,\ q,\ H \times W)$
// Iterating the new 5-D chaotic system for $H \times W$ times and generates five sequences
// Permutation process
$SR \leftarrow fix(mod(Y1(1:H) \times 10^{16},\ W-1)) + 1$ // Generates an integer sequence of length H utilized for circular shift the elements of each row
$SC \leftarrow fix(mod(Y2(1:W) \times 10^{16},\ H-1)) + 1$ // Generates an integer sequence of length W utilized for circular shift the elements of each column
// Circular shift right for the elements of each row
for $i \leftarrow 1$ *to* H **do**
  for $j \leftarrow 1$ *to* W **do**
    $pos \leftarrow SR(i) + j \mod W$
    if *pos==0* **then**
      $pos \leftarrow W$
    $SRIm(i, pos, :) \leftarrow PIm(i, j, :)$
// Circular shift right for the elements of each column
for $i \leftarrow 1$ *to* H **do**
  for $j \leftarrow 1$ *to* W **do**
    $pos \leftarrow SC(j) + i \mod H$
    if *pos==0* **then**
      $pos \leftarrow H$
    $PerIm(pos, j, :) \leftarrow SRIm(i, j, :)$
// Substitution process
$K1(:,1) \leftarrow reshape(fix(Y3 \times 10^{16} \mod 256), H, W)$ // Converting Y3 sequence into integer values and reshape the outcome to a matrix of dimensional $H \times W$
$K1(:,2) \leftarrow reshape(fix(Y4 \times 10^{16} \mod 256), H, W)$
$K1(:,3) \leftarrow reshape(fix(Y5 \times 10^{16} \mod 256), H, W)$
$SubIm \leftarrow PerIm \oplus K1$
// Update initial conditions
$PixSum \leftarrow \sum_{h\leftarrow 1}^{H} \sum_{w\leftarrow 1}^{W} \sum_{l\leftarrow 1}^{L} SubIm(h, w, l)$
$Delta \leftarrow \frac{PixSum \mod 512}{512} \times 0.5$
$y1_0 = 0.5 \times y1_0 + Delta$
$y2_0 = 0.5 \times y2_0 + Delta$
$y3_0 = 0.5 \times y3_0 + Delta$
$y4_0 = 0.5 \times y4_0 + Delta$
$y5_0 = 0.5 \times y5_0 + Delta$
$[Y1\ \ Y2\ \ Y3\ \ Y4\ \ Y5] \leftarrow new\ 5D\ chaotic\ system(y1_0,\ y2_0,\ y3_0,\ y4_0,\ y5_0,\ a,\ b,\ c,\ d,\ p,\ q,\ H \times W)$
$K2(:,1) \leftarrow reshape(fix(Y1 \times 10^{16} \mod 256), H, W)$
$K2(:,2) \leftarrow reshape(fix(Y2 \times 10^{16} \mod 256), H, W)$
$K2(:,3) \leftarrow reshape(fix(Y3 \times 10^{16} \mod 256), H, W)$
$CIm \leftarrow SubIm \oplus K2$// Cipher-image

mathematically as follows:

$$E(X) = -\sum_{i=0}^{255} p(x_i) \log_2 \left(p(x_i)\right) \tag{17}$$

where $p(x_i)$ indicates to the probability of x_i. The potential values for a greyscale image are 2^8, therefore the typical entropy value is 8-bit. Therefore, to confirm the effectiveness of the given approach, the entropy value of the ciphered

This article has been accepted for publication in a future issue of this journal, but has not been fully edited. Content may change prior to final publication. Citation information: DOI 10.1109/ACCESS.2021.3085483, IEEE Access

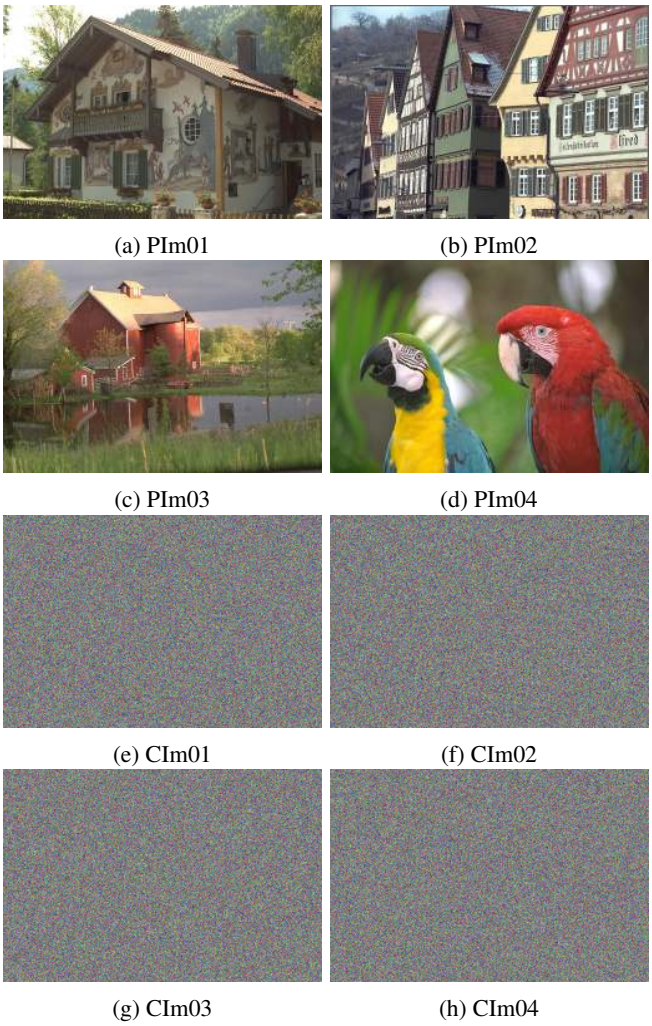

(a) PIm01 (b) PIm02

(c) PIm03 (d) PIm04

(e) CIm01 (f) CIm02

(g) CIm03 (h) CIm04

FIGURE 17: Experimental dataset of images, which the first two rows indicate the plain images and it's corresponding ciphered ones are provided in the last two rows.

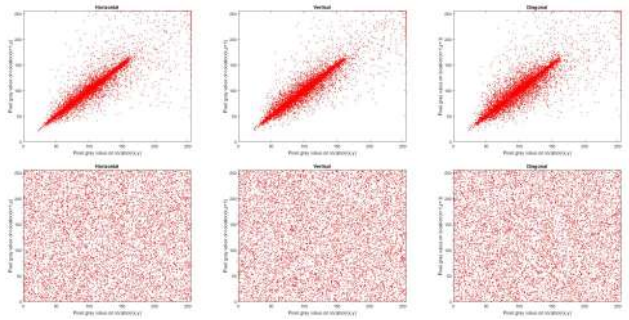

FIGURE 18: Distributions of C_{pc} values for the red component of image Im01, where the first row denotes the red component of PIm01 and the second row denotes the red component of image CIm01.

images must be nearby 8. Nevertheless, the global entropy neglects to evaluate the true randomness for ciphered images. Accordingly, local entropy can be calculated by the average

TABLE 4: Outcomes of C_{pc} for the experimented dataset

image	Colour component	direction		
		Hor.	Ver.	Dia.
PIm01	R	0.93001	0.94081	0.90786
	G	0.92888	0.93767	0.90242
	B	0.91587	0.92604	0.89211
CIm01	R	-0.00038	0.00058	-0.00071
	G	-0.00011	0.00112	0.00038
	B	-0.00098	0.00071	-0.00086
PIm02	R	0.92245	0.87761	0.81083
	G	0.92683	0.88951	0.82543
	B	0.90351	0.86175	0.77601
CIm02	R	-0.00072	0.00092	0.00052
	G	-0.00024	-0.00083	0.00061
	B	-0.00031	-0.00035	-0.00082
PIm03	R	0.96227	0.95549	0.93653
	G	0.95137	0.94483	0.91863
	B	0.96153	0.95619	0.93319
CIm03	R	-0.00002	-0.00107	-0.00065
	G	-0.00014	0.00122	-0.00029
	B	-0.00048	0.00013	0.00107
PIm04	R	0.98521	0.98794	0.97978
	G	0.98308	0.98529	0.97552
	B	0.98567	0.98775	0.97918
CIm04	R	-0.00032	-0.00085	0.00084
	G	0.00096	0.00002	0.00127
	B	-0.00068	0.00038	0.00089

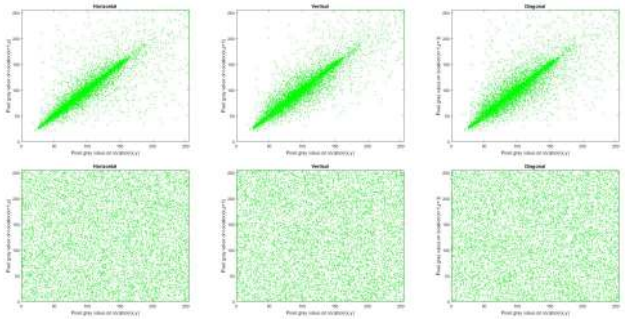

FIGURE 19: Distributions of C_{pc} values for the green component of image Im01, where the first row denotes the green component of PIm01 and the second row denotes the green component of image CIm01.

TABLE 5: NPCR and UACI values for experimented dataset

Image	NPCR %	UACI %
Im01	99.60267	33.42806
Im02	99.60742	33.47349
Im03	99.60064	33.44653
Im04	99.60369	33.48648

of global entropies over all the non-overlapping blocks (per block has 1936 pixels) [48]. Table 7 presented the values of global and local information entropies for the plain images and their corresponding ciphered ones, which all values of information entropy for ciphered images are very near to 8-bit. Therefore, the presented mechanism is secure against entropy attack.

This article has been accepted for publication in a future issue of this journal, but has not been fully edited. Content may change prior to final publication. Citation information: DOI 10.1109/ACCESS.2021.3085483, IEEE Access

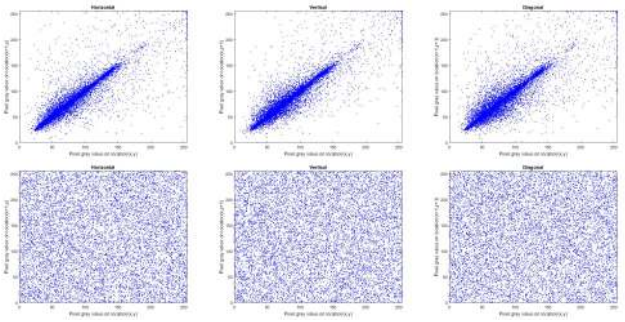

FIGURE 20: Distributions of C_{pc} values for the blue component of image Im01, where the first row denotes the blue component of PIm01 and the second row denotes the blue component of image CIm01.

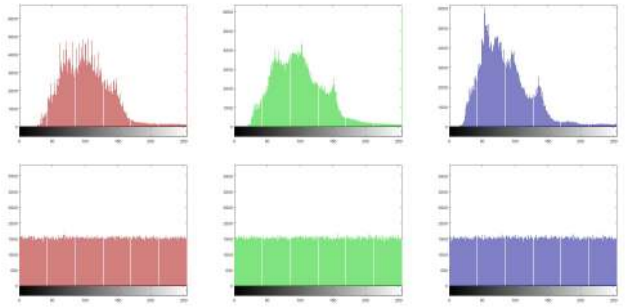

FIGURE 21: Histograms of Im01, where the first row indicates to the Histograms of PIm01 and the second row denotes the Histograms of CIm01 image.

TABLE 6: χ^2 values for our proposed approach

Image	Chi-square value			Outcome
	R	G	B	
PIm01	817766.501	677362.427	616936.171	Not uniform
PIm02	285277.463	219680.628	221228.608	Not uniform
PIm03	503535.636	368802.614	490511.246	Not uniform
PIm04	303687.966	254324.451	603349.493	Not uniform
CIm01	291.0885	244.0794	268.4153	Uniform
CIm02	243.8124	234.8763	256.3124	Uniform
CIm03	258.5377	243.6536	272.5638	Uniform
CIm04	262.6718	240.3085	271.4869	Uniform

TABLE 7: Global and local information entropies for our encryption approach

Image	Global		Local	
	Plain	cipher	Plain	cipher
Im01	7.136653	7.999832	5.673345	7.901366
Im02	7.673795	7.999851	6.552062	7.902948
Im03	7.385258	7.999844	5.590770	7.902664
Im04	7.601941	7.999845	5.396978	7.902361

E. OCCLUSION ATTACKS

If data is transmitted via communication channels, noise can affect the transmitted information and lose some of its parts ([49], [50]). Therefore, a highly designed cryptographic system should be able to withstand data loss attacks. To assess the proposed encryption approach towards the loss of information, we execute an occlusion analysis by cutting out some of the data in the encrypted image or append noise to it and then trying to retrieve the secret image from the defective cipher image via the deciphering process. Figs. 22 and 23 present the results of occlusion attacks in which the plain image is effectively retrieved during the deciphering process.

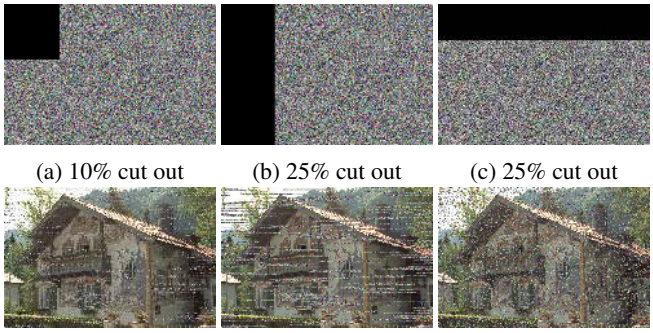

(a) 10% cut out (b) 25% cut out (c) 25% cut out

FIGURE 22: Data loss attack. The first row indicates the defective cipher images via cutting out some part data and the second row represents the corresponding decrypted ones.

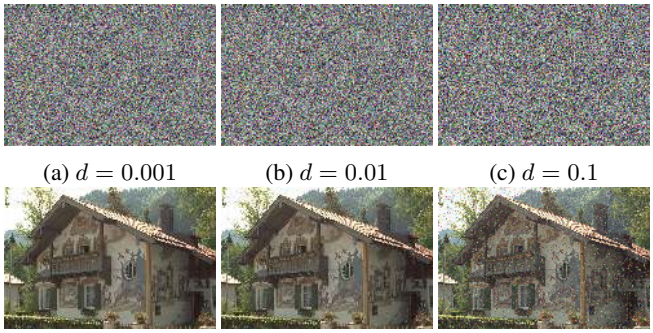

(a) $d = 0.001$ (b) $d = 0.01$ (c) $d = 0.1$

FIGURE 23: Noise attack. The first row indicates the defective cipher images via varying Salt & Pepper noise density and the second row represents the corresponding decrypted ones.

F. KEY SENSITIVITY ANALYSES

The sensitivity of the key is utilised to ensure the security of the cryptosystem. To assess the key sensitivity of the proposed mechanism, CIm01 image is deciphered by slight changes in the cryptographic key, as shown in Figure 24.

G. COMPARATIVE ANALYSIS

To confirm the effectiveness of the proposed encryption approach in relation to other very recently approaches ([47], [48], [50]), Table 8 presents a simple comparison of the proposed approach with other related methods in terms of correlation coefficients, NPCR, UACI, global and local information entropy, and Chi-square test. The values provided in Table 8 confirms the effectiveness of the presented mechanism.

This article has been accepted for publication in a future issue of this journal, but has not been fully edited. Content may change prior to final publication. Citation information: DOI 10.1109/ACCESS.2021.3085483, IEEE Access

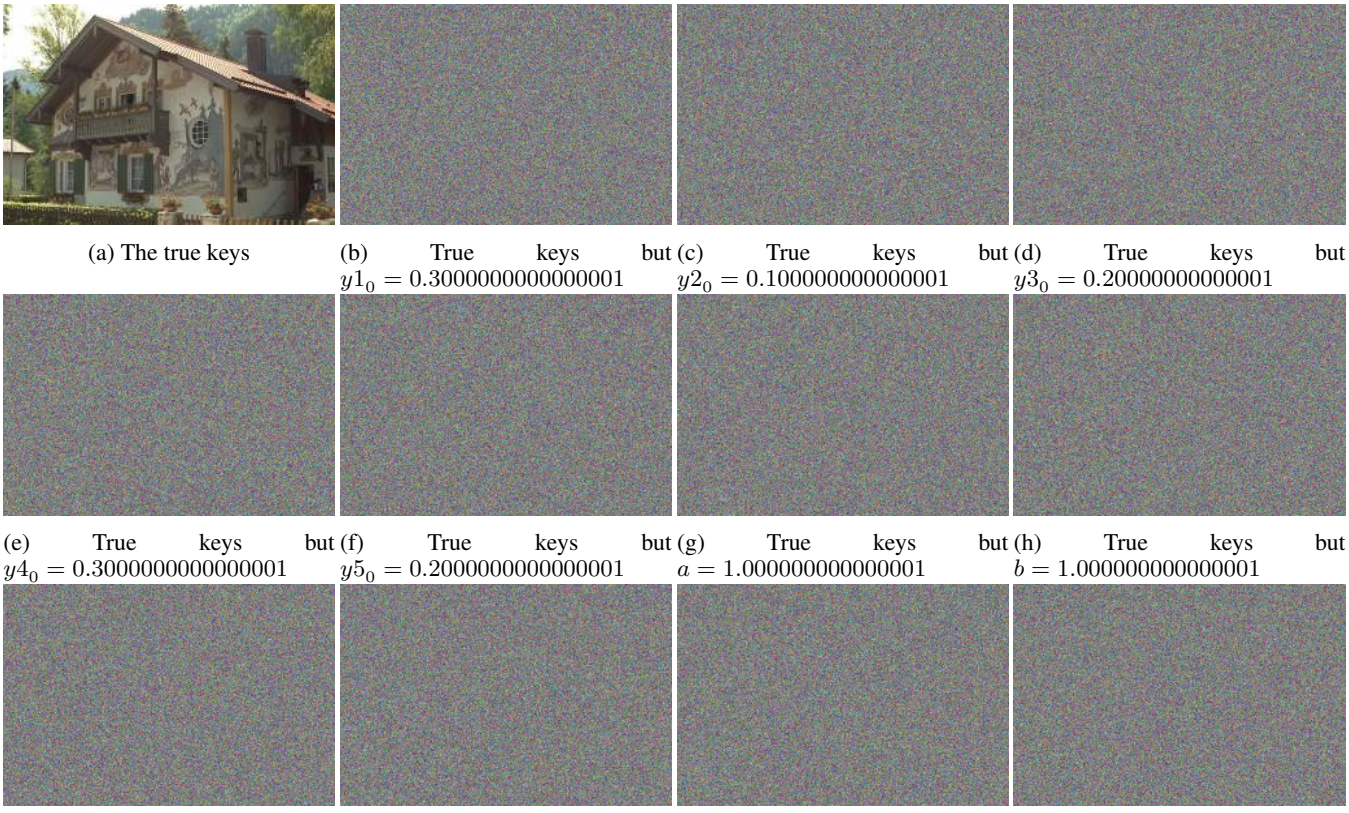

(a) The true keys (b) True keys but $y1_0 = 0.3000000000000001$ (c) True keys but $y2_0 = 0.100000000000001$ (d) True keys but $y3_0 = 0.20000000000001$

(e) True keys but $y4_0 = 0.3000000000000001$ (f) True keys but $y5_0 = 0.2000000000000001$ (g) True keys but $a = 1.000000000000001$ (h) True keys but $b = 1.000000000000001$

(i) True keys but $c = 5.000000000000001$ (j) True keys but $d = 6.000000000000001$ (k) True keys but $p = 6.000000000000001$ (l) True keys but $q = 8.000000000000001$

FIGURE 24: Decrypting image Im01 with slight changes in key parameters.

TABLE 8: Comparison of the presented strategy with other similar strategies in terms of average values of correlation coefficients, NPCR, UACI, global and local information entropy, and Chi-square test.

Approach	Correlation			Entropy		NPCR%	UACI%	χ^2-test
	Hor.	Ver.	Dia.	Global	Local			
Our	-0.00028	0.00016	0.00018	7.99984	7.90236	99.6036	33.4586	257.3172
Ref. [47]	-0.0042	-0.0049	-0.0045	7.9995	7.9030	99.6101	33.5252	249.8444
Ref. [48]	0.00001	0.000921	-0.00072	7.99721	7.90268	99.6146	33.5136	252.9779
Ref. [50]	0.0002	0.0001	-0.0001	7.99976	7.90259	99.6058	-	256.3767

VIII. CONCLUSIONS

This work described the modelling, circuit design and engineering applications of a new 5-D hyperchaotic dynamo system, which was constructed by adding two feedback controllers to the Rikitake 2-disk dynamo system (1958). It was shown that the new 5-D hyperchaotic system does not possess any equilibrium point and deduce that the new 5-D system has a hidden hyperchaotic attractor. Using Multisim, an electronic circuit design was designed for the new 5-D hyperchaotic dynamo system for practical applications. The FPGA implementation of the new 5-D hyper-chaotic dynamo system was performed by applying three numerical methods, all of them showing good agreement to MatLab simulations by using 32 bit. To increase accuracy one just can increase the number of bits in the FPGA but at the cost of sacrifying power consumption. As an application, we devise a dual core high speed hybrid true random number generator (TRNG) using Ring and Heun algorithm based on the new 5-D hyperchaotic oscillator on FPGA. Finally, based on the hyperchaotic behaviour of our new 5-D hyperchaotic dynamo system, we proposed a new image encryption approach. Experimental outcomes of the presented encryption approach confirmed that our 5-D hyperchaotic system has good cryptographic properties and its usability in various cryptographic applications.

.

REFERENCES

[1] O. E. Rössler and C. Letellier, Chaos: The World of Nonperiodic Oscillations. Berlin, Germany: Springer, 2020.

[2] J. Singh, K. Lochan, and B. Roy, "Secure communication using a new hyperchaotic system with hidden attractors," Lecture Notes in Electrical Engineering, vol. 581, pp. 67–79, 2020.

[3] X. An, M. Jiang, W. Deng, and J. Fang, "A novel dual memristor hyperchaotic system and its application for secure communication based on three-fold function projection synchronization," International Journal of Numerical Modelling: Electronic Networks, Devices and Fields, vol. 34, no. 2, 2021, Article ID 2825.

[4] A. Ouannas, A. Karouma, G. Grassi, V.-T. Pham, and V. Luong, "A novel secure communications scheme based on chaotic modulation, recursive encryption and chaotic masking," Alexandria Engineering Journal, vol. 60, no. 1, pp. 1873–1884, 2021.

[5] M. Sahin, H. Guler, and S. Hamamci, "Design and realization of a hyperchaotic memristive system for communication system on FPGA," Traitement du Signal, vol. 37, no. 6, pp. 939–953, 2020.

[6] F. Yang, J. Mou, Y. Cao, and R. Chu, "An image encryption algorithm based on bp neural network and hyperchaotic system," China Communications, vol. 17, no. 5, pp. 21–28, 2020.

[7] M. Ahmad, M. Doja, and M. Beg, "Security analysis and enhancements of an image cryptosystem based on hyperchaotic system," Journal of King Saud University - Computer and Information Sciences, vol. 33, no. 1, pp. 77–85, 2021.

[8] C. Zhong and M.-S. Pan, "Encryption algorithm based on scrambling substitution of new hyperchaotic Chen system," Chinese Journal of Liquid Crystals and Displays, vol. 35, no. 1, pp. 91–97, 2020.

[9] S. Vaidyanathan, A. Azar, A. Akgul, C.-H. Lien, S. Kacar, and U. Cavusoglu, "A memristor-based system with hidden hyperchaotic attractors, its circuit design, synchronisation via integral sliding mode control and an application to voice encryption," International Journal of Automation and Control, vol. 13, no. 6, pp. 644–667, 2019.

[10] D. Fang and S. Sun, "A new scheme for image steganography based on hyperchaotic map and DNA sequence," Journal of Information Hiding and Multimedia Signal Processing, vol. 9, no. 2, pp. 392–399, 2018.

[11] Q. Yang, L. Yang, and B. Ou, "Hidden hyperchaotic attractors in a new 5D system based on chaotic System with two stable node-foci," International Journal of Bifurcation and Chaos, vol. 29, no. 7, 2019, Article ID 1950092.

[12] J. Singh, K. Rajagopal, and B. Roy, "A new 5D hyperchaotic system with stable equilibrium point, transient chaotic behaviour and its fractional-order form," Pramana - Journal of Physics, vol. 91, no. 3, 2018, Article ID 33.

[13] F. Zhang, R. Chen, X. Wang, X. Chen, C. Mu, and X. Liao, "Dynamics of a new 5D hyperchaotic system of Lorenz type," International Journal of Bifurcation and Chaos, vol. 28, no. 3, 2018, Article ID 1850036.

[14] R. Wang, M. Li, Z. Gao, and H. Sun, "A new memristor-based 5D chaotic system and circuit implementation," Complexity, vol. 2018, 2018, Article ID 6069401.

[15] I. Koyuncu, M. Alcin, M. Tuna, I. Pehlivan, M. Varan, and S. Vaidyanathan, "Real-time high-speed 5-d hyperchaotic lorenz system on fpga," International Journal of Computer Applications in Technology, vol. 61, no. 3, pp. 152–165, 2019.

[16] D. Dudkowski, S. Jafari, K. T., N. Kuznetsov, G. Leonov, and A. Prasad, "Hidden attractors in dynamical systems," Physics Reports, vol. 637, pp. 1–50, 2016.

[17] D. Dudkowski, A. Prasad, and T. Kapitaniak, "Perpetual points and hidden attractors in dynamical systems," Physics Letters A, vol. 379, pp. 2591—-2596, 2015.

[18] T. Rikitake, "Oscillations of a system of disk dynamos," Mathematical Proceedings of the Cambridge Philosophical Society, vol. 54, pp. 89–105, 1958.

[19] A. Sambas, S. Vaidyanathan, S. Zhang, Y. Zeng, M. Mohamed, and M. Mamat, "A new double-wing chaotic system with coexisting attractors and line equilibrium: Bifurcation analysis and electronic circuit simulation," IEEE Access, vol. 7, pp. 115 454–115 462, 2019.

[20] A. Sambas, M. Mamat, A. Arafa, G. Mahmoud, M. Mohamed, and W. Sanjaya, "A new chaotic system with line of equilibria: Dynamics, passive control and circuit design," International Journal of Electrical and Computer Engineering, vol. 9, no. 4, pp. 2336–2345, 2019.

[21] S. Vaidyanathan, A. Sambas, S. Zhang, Y. Zeng, M. Mohamed, and M. Mamat, "A new two-scroll chaotic system with two nonlinearities: Dynamical analysis and circuit simulation," Telkomnika (Telecommunication Computing Electronics and Control), vol. 17, no. 5, pp. 2465–2474, 2019.

[22] A. Sambas, S. Vaidyanathan, I. Moroz, B. Idowu, M. Mohamed, M. Mamat, and W. Sanjaya, "A simple multi-stable chaotic jerk system with two saddle-foci equilibrium points: Analysis, synchronization via backstepping technique and MultiSim circuit design," International Journal of Electrical and Computer Engineering, vol. 11, no. 4, pp. 2941–2952, 2021.

[23] E. Tlelo-Cuautle, A. D. Pano-Azucena, O. Guillén-Fernández, and A. Silva-Juárez, Analog/Digital Implementation of Fractional Order Chaotic Circuits and Applications. Berlin, Germany: Springer, 2020.

[24] I. Koyuncu, M. Alcin, M. Tuna, I. Pehlivan, M. Varan, and S. Vaidyanathan, "Real-time high-speed 5-D hyperchaotic Lorenz system on FPGA," International Journal of Computer Applications in Technology, vol. 61, no. 3, pp. 152–165, 2019.

[25] M. Tuna, M. Alcin, I. Koyuncu, C. B. Fidan, and I. Pehlivan, "High speed FPGA-based chaotic oscillator design," Microprocessors and Microsystems, vol. 66, pp. 72–80, 2019.

[26] I. Koyuncu and H. I. Seker, "Implementation of Dormand-Prince based chaotic oscillator designs in different IQ-Math number standards on FPGA," Sakarya University Journal of Science, vol. 23, no. 5, pp. 859–868, 2019.

[27] S. Vaidyanathan, I. Pehlivan, L. G. Dolvis, K. Jacques, M. Alcin, M. Tuna, and I. Koyuncu, "A novel ANN-based four-dimensional two-disk hyperchaotic dynamical system, bifurcation analysis, circuit realisation and FPGA based TRNG implementation," International Journal of Computer Applications in Technology, vol. 62, no. 1, pp. 20–35, 2020.

[28] I. Koyuncu, M. Alcin, P. Erdogmus, and M. Tuna, "Artificial neural network-based 4-D hyper-chaotic system on field programmable gate array," International Journal of Intelligent Systems and Applications in Engineering, vol. 8, no. 2, pp. 102–108, 2020.

[29] M. Tuna, A. Karthikeyan, K. Rajagopal, M. Alcin, and I. Koyuncu, "Hyperjerk multiscroll oscillators with megastability: Analysis, FPGA implementation and a novel ANN-ring-based True Random Number Generator," AEU-International Journal of Electronics and Communications, vol. 112, 2019, article ID 152941.

[30] K. Rajagopal, M. Tuna, A. Karthikeyan, I. Koyuncu, P. Duraisamy, and A. Akgul, "Dynamical analysis, sliding mode synchronization of a fractional-order memristor Hopfield neural network with parameter uncertainties and its non-fractional-order FPGA implementation," The European Physical Journal Special Topics, vol. 228, no. 10, pp. 2065–2080, 2019.

[31] M. Alcin, I. Koyuncu, M. Tuna, M. Varan, and I. Pehlivan, "A novel high speed artificial neural network-based chaotic true random number generator on field programmable gate array," International Journal of Circuit Theory and Applications, vol. 47, no. 3, pp. 365–378, 2019.

[32] M. Tuna and C. B. Fidan, "A study on the importance of chaotic oscillators based on FPGA for true random number generating (TRNG) and chaotic systems," Journal of the Faculty of Engineering and Architecture of Gazi University, vol. 33, no. 2, pp. 469–486, 2018.

[33] I. Koyuncu, M. Tuna, I. Pehlivan, C. B. Fidan, and M. Alcın, "Design, FPGA implementation and statistical analysis of chaos-ring based dual entropy core true random number generator," Analog Integrated Circuits and Signal Processing, vol. 102, no. 2, pp. 445–456, 2020.

[34] B. Abd-El-Atty, A. M. Elias, A. Alanezi, and A. A. Abd El-Latif, "Optical image encryption based on quantum walks," Optics and Lasers in Engineering, 2020.

[35] A. A. A. El-Latif, B. Abd-El-Atty, W. Mazurczyk, C. Fung, and S. E. Venegas-Andraca, "Secure data encryption based on quantum walks for 5g internet of things scenario," IEEE Transactions on Network and Service Management, vol. 17, no. 1, pp. 118–131, mar 2020.

[36] B. Abd-El-Atty, M. Amin, A. Abd-El-Latif, H. Ugail, and I. Mehmood, "An efficient cryptosystem based on the logistic-chebyshev map," in 2019 13th International Conference on Software, Knowledge, Information Management and Applications (SKIMA). IEEE, 2019, pp. 1–6.

[37] A. A. A. El-Latif, B. Abd-El-Atty, S. Elseuofi, H. S. Khalifa, A. S. Alghamdi, K. Polat, and M. Amin, "Secret images transfer in cloud system based on investigating quantum walks in steganography approaches," Physica A: Statistical Mechanics and its Applications, vol. 541, p. 123687, mar 2020.

[38] A. A. A. EL-Latif, B. Abd-El-Atty, and S. E. Venegas-Andraca, "Controlled alternate quantum walk-based pseudo-random number generator and its application to quantum color image encryption," Physica A: Statistical Mechanics and its Applications, vol. 547, p. 123869, jun 2020.

[39] S. Vaidyanathan, I. Pehlivan, L. G. Dolvis, K. Jacques, M. Alcin, M. Tuna, and I. Koyuncu, "A novel ANN-based four-dimensional two-disk hyperchaotic dynamical system, bifurcation analysis, circuit realisation and FPGA-based TRNG implementation," International Journal of Computer Applications in Technology, vol. 62, no. 1, pp. 20–35, 2020.

[40] S. Zhang, X. Wang, and Z. Zeng, "A simple no-equilibrium chaotic system with only one signum function for generating multidirectional variable hidden attractors and its hardware implementation," Chaos, vol. 30, no. 5, 2020, Article ID 053129.

[41] S. Zhang, J. Zheng, X. Wang, Z. Zeng, and S. He, "Initial offset boosting coexisting attractors in memristive multi-double-scroll Hopfield neural network," Nonlinear Dynamics, vol. 62, pp. 2821–2841, 2020.
[42] B. Karakaya, A. Gülten, and M. Frasca, "A true random bit generator based on a memristive chaotic circuit: Analysis, design and fpga implementation," Chaos, Solitons & Fractals, vol. 119, pp. 143–149, 2019.
[43] "True color kodak images," http://r0k.us/graphics/kodak/, accessed: 2020-9-30.
[44] A. A. A. El-Latif, B. Abd-El-Atty, M. Amin, and A. M. Iliyasu, "Quantum-inspired cascaded discrete-time quantum walks with induced chaotic dynamics and cryptographic applications," Scientific Reports, vol. 10, no. 1, feb 2020.
[45] A. A. A. EL-Latif, B. Abd-El-Atty, E. M. Abou-Nassar, and S. E. Venegas-Andraca, "Controlled alternate quantum walks based privacy preserving healthcare images in internet of things," Optics & Laser Technology, vol. 124, p. 105942, apr 2020.
[46] B. Abd-El-Atty, A. A. A. El-Latif, and S. E. Venegas-Andraca, "An encryption protocol for NEQR images based on one-particle quantum walks on a circle," Quantum Information Processing, vol. 18, no. 9, jul 2019.
[47] N. Tsafack, J. Kengne, B. Abd-El-Atty, A. M. Iliyasu, K. Hirota, and A. A. A. EL-Latif, "Design and implementation of a simple dynamical 4-d chaotic circuit with applications in image encryption," Information Sciences, vol. 515, pp. 191–217, 2020.
[48] N. Tsafack, S. Sankar, B. Abd-El-Atty, J. Kengne, K. Jithin, A. Belazi, I. Mehmood, A. K. Bashir, O.-Y. Song, and A. A. Abd El-Latif, "A new chaotic map with dynamic analysis and encryption application in internet of health things," IEEE Access, vol. 8, pp. 137 731–137 744, 2020.
[49] B. Abd-El-Atty, A. M. Iliyasu, H. Alaskar, A. El-Latif, and A. Ahmed, "A robust quasi-quantum walks-based steganography protocol for secure transmission of images on cloud-based e-healthcare platforms," Sensors, vol. 20, no. 11, p. 3108, 2020.
[50] A. Sambas, S. Vaidyanathan, E. Tlelo-Cuautle, B. Abd-El-Atty, A. A. Abd El-Latif, O. Guillén-Fernández, Y. Hidayat, G. Gundara et al., "A 3-D multi-stable system with a peanut-shaped equilibrium curve: Circuit design, FPGA realization, and an application to image encryption," IEEE Access, vol. 8, pp. 137 116–137 132, 2020.

SUNDARAPANDIAN VAIDYANATHAN received the D.Sc. degree in Electrical and Systems Engineering from Washington University at St. Louis, St. Louis, MO, USA, in 1996. He is currently a Professor and Dean with the Research and Development Centre, Vel Tech University, Chennai, India. He has published over 500 Scopus-indexed research publications. His current research interests include control systems, chaos theory, intelligent control, optimal control, fractional order systems, mathematical modeling, and scientific computing.

ACENG SAMBAS received the M.Sc. degree in Mathematics from Universiti Sultan Zainal Abidin (UniSZA), Malaysia, in 2015. He has been a Lecturer with the Muhammadiyah University of Tasikmalaya, Indonesia, since 2015. His current research interests include dynamical systems, chaotic signals, electrical engineering, computational science, signal processing, robotics, embedded systems, and artificial intelligence.

ESTEBAN TLELO-CUAUTLE received a B.Sc. degree from Instituto Tecnológico de Puebla México in 1993. He then received both M.Sc. and Ph.D. degrees from Instituto Nacional de Astrofísica, Óptica y Electrónica (INAOE), México in 1995 and 2000, respectively. In 2001 he was appointed as Professor-Researcher at INAOE. He has authored 4 books, edited 11 books and around 300 works published in book chapters, international journals and conferences. He serves as Associate Editor in IEEE Trans on Circuits and Systems I: Regular Papers, Engineering Applications of Artificial Intelligence, Electronics, Integration the VLSI Journal, PLOS ONE, and Frontiers of Information Technology and Electronics Engineering. His research interests include analog signal processing, synthesis and design of integrated circuits, optimization by metaheuristics, design and applications of chaotic systems, security in the internet of things, symbolic analysis and analog/RF and mixed-signal design automation tools.

BASSEM ABD-EL-ATTY received B.S. degree in physics and computer science, M.Sc. degree in computer science, and Ph.D degree in computer science all from Menoufia University, Egypt, in 2010, 2017, and 2020 respectively. He is author and co-author of more than 20 papers, including refereed IEEE/Springer/Elsevier journals, conference papers, and book chapters. He is a reviewer in a set of reputable journals in Elsevier and Springer His research interests include quantum information processing and image processing.

AHMED A. ABD EL-LATIF received the B.Sc. degree with honor rank in Mathematics and Computer Science in 2005 and M.Sc. degree in Computer Science in 2010, all from Menoufia University, Egypt. The Ph. D. degree in Computer Science & Technology from Harbin Institute of Technology (H.I.T), China in 2013. He is an Associate Professor at the Menoufia University in Egypt. He has published 120 papers in refereed international SCI-IF journals. Reviewer of many prestigious and reputed journals. He received many national and international awards such as State Encouragement Award in Engineering Sciences 2016, Arab Republic of Egypt, etc. He is a fellow at Academy of Scientific Research and Technology, Egypt. His areas of interests are multimedia content encryption, secure wireless communication, IoT, applied cryptanalysis, perceptual cryptography, secret media sharing, information hiding, biometrics, forensic analysis in digital images, and quantum information processing.

OMAR GUILLÉN-FERNÁNDEZ received a Bachelor degree from Instituto Tecnológico de Veracruz in 2015, and the M.Sc. degree in Electronics from Instituto Nacional de Astrofísica, Óptica y Electrónica (INAOE) at México, in 2018. He is currently pursuing his Ph.D. degree at INAOE. He has authored one book and one book chapter, and published five journal papers and a couple of conference proceedings. His topics of interest are oriented to chaotic systems, synchronization techniques, security, embedded systems, optimization and integrated circuit design and applications.

This article has been accepted for publication in a future issue of this journal, but has not been fully edited. Content may change prior to final publication. Citation information: DOI 10.1109/ACCESS.2021.3085483, IEEE Access

MUSTAFA MAMAT is currently a Professor and the Dean of Graduate School at Universiti Sultan Zainal Abidin (UniSZA), Malaysia since 2013. He was first appointed as a Lecturer at the Universiti Malaysia Terengganu (UMT) in 1999. He obtained his PhD from the UMT in 2007 with specialization in optimization. Later on, he was appointed as a Senior Lecturer in 2008 and then as an Associate Professor in 2010 also at the UMT. To date, he has successfully supervised more than 60 postgraduate students and published more than 150 research papers in various international journals and conferences. His research interests include conjugate gradient methods, steepest descent methods, Broydens family and quasi-Newton methods.

MOHAMAD AFENDEE MOHAMED received his PhD in Mathematical Cryptography in 2011 and currently serves as an associate professor at Universiti Sultan Zainal Abidin. His research interests include both theoretical and application issues in the domain of data security, and mobile and wireless networking.

MURAT ALÇIN received the BSc, MSc and PhD degrees in Electronic-Computer Teaching from the University of Marmara, Turkey, in 2006 and in 2009, and department of Electrical and Electronics Engineering at Sakarya University, in Sakarya-Turkey, 2017, respectively. From 2008 to 2012, he was an instructor in Abant İzzet Baysal University Electronic Technology Program at Bolu Vocational School, Bolu-Turkey. Since 2018, he is an Assistant Professor in the Department of Mechatronics Engineering at Afyon Kocatepe University, in Afyon-Turkey. His research interests include neural networks, chaotic systems and FPGA-based digital system design.

MURAT TUNA received his BSc and MSc in Electrical Education from Kocaeli University of Technical Education, in 2004, and Kocaeli University of Institute of Science, Kocaeli, Turkey, in 2008. He received his PhD in the Department of Electrical and Electronics Engineering at Karabuk University, Karabuk-Turkey in 2017. Currently, he is working at Kirklareli University in Turkey, Assistant Professor, since 2009. His main research topics include chaos, TRNG, FPGA-based digital system design and reconfigurable computing. He is also interested in mathematical model and control of nonlinear systems.

İHSAN PEHLIVAN .received the B.S. from Istanbul Technical University in 1997, M.S. and PhD degrees in 2001 and 2007 respectively in Electrical-Electronic Engineering from Sakarya University, Sakarya-Turkey. He is an Professor in the Department of Electrical and Electronics Engineering at Sakarya Applied Sciences University, in Sakarya-Turkey. He is the author of a book, and published more than 30 articles. His research interests include chaos, electric circuits and signals-system.

İSMAIL KOYUNCU has an MSc from Abant Izzet Baysal University, Bolu-Turkey. He completed his doctoral research in the Department of Electrical and Electronics Engineering at Sakarya University, Sakarya-Turkey in 2014. Since 2017, he is an Assocate Professor in the Department of Electric-Electronic Engineering at Afyon Kocatepe University, in Afyon-Turkey. His main research interests are FPGA-based digital system design, chaos, TRNG and reconfigurable computing. He is also interested in FPGA-based artificial neural networks and computer graphics.

MOHD ASRUL HERY IBRAHIM was born in Kelantan, Malaysia. He received the B.Sc degree in Financial Mathematics from the Universiti Malaysia Terengganu, Malaysia and M.Sc degree in Applied Mathematics from the same university. He also doing Ph.D degree in Universiti Sultan Zainal Abidin, major in Mathematical Sciences. His current research interests include optimization, Numerical Analysis, Business mathematics and Business Statistics. He writes regularly and has published more than 50 scientific articles in journals, and conferences.